CrossMark

ORIGINAL PAPER

Climate change impact on precipitation and cardinal temperatures in different climatic zones in Iran: analyzing the probable effects on cereal water-use efficiency

Fatemeh Karandish[1] · Seyed Saeed Mousavi[1] · Hossein Tabari[2]

Abstract Global greenhouse gases increase could be a threat to sustainable agriculture since it might affect both green water and air temperature. Using the outputs of 15 general circulation models (GCMs) under three SRES scenarios of A1B, A2 and B1, the projected annual and seasonal precipitation (P) and cardinal temperatures (T) were analyzed for five climatic zones in Iran. In addition, the probable effects of climate change on cereal production were studied using AquaCrop model. Data obtained from the GCMs were downscaled using LARS-WG for 52 synoptic stations up to 2100. An uncertainty analysis was done for the projected P and T associated to GCMs and SRES scenarios. Based on station observations, LARS-WG was capable enough for simulating both P and T for all the climatic zones. The majority of GCMs as well as the median of the ensemble for each scenario project positive P and T changes. In all the climatic zones, wet seasons have a higher P increase than dry seasons, with the highest increase (27.9–83.3%) corresponding to hyper-arid and arid regions. A few GCMs project a P reduction mainly in Mediterranean and hyper-humid climatic regions. The highest increase (11.2–44.5%) in minimum T occurred in Mediterranean climatic regions followed by semi-arid regions in which a concurrent increase in maximum T (2.9–14.6%) occurred. The largest uncertainty in P and cardinal T projection occurred in rainy seasons as well as in hyper-humid regions. The AquaCrop simulation results revealed that the increased cardinal T under global warming will cause 0–28.5% increase in cereal water requirement as well as 0–15% reduction in crop yield leading to 0–30% reduction in water use efficiency in 95% of the country.

Keywords AquaCrop model · Climatic zones · Future climate conditions · GCMs · SRES scenarios · LARS-WG · Uncertainty analysis

1 Introduction

There is a solid agreement among scientists that a genetic evolution occurred in the Earth's climate related to increases in atmospheric CO_2 and other radiatively active gases, leading to a climate change (Tabari et al. 2011). Climate change is defined as any systematic change in the long-term (several decades or longer) evolution describing the climate system (Gil-Alana 2012). Over the recent 100-year period (1906–2005), a global surface warming at a rate of 0.74 ± 0.18 °C has been taking place and the warming rate over the second half of this period is almost twice as that of the whole 100-year period (IPCC 2007). The global warming might affect various meteorological variables such as precipitation and temperature (Tabari et al. 2015; Yu et al. 2002; Haskett et al. 2000). Many studies have clearly shown the variability of climatic variables in Southwest Asia as a result of human interference in the ecosystems (e.g., Tabari and Hosseinzadeh

✉ Fatemeh Karandish
  Karandish_h@yahoo.com; F.Karandish@uoz.ac.ir

  Seyed Saeed Mousavi
  saeedmoosavi8@yahoo.com

  Hossein Tabari
  tabari.ho@gmail.com; hossein.tabari@bwk.kuleuven.be

[1] Water Engineering Department, University of Zabol, Zabol, Iran

[2] Hydraulics Division, Department of Civil Engineering, KU Leuven, Louvain, Belgium

Talaee 2011; Hamdi et al. 2009; Smadi 2006; Evans and Geerken 2004; Abahussain et al. 2002).

Any change in meteorological variables due to climate change will affect both water and food security since some of them such as precipitation and air temperature (T) are key factors in agriculture. In rainfed agriculture, precipitation is the only water resource which supplies crop water requirement during the growing season. Even for irrigated agriculture, green water plays a major role in economic agriculture since applying blue water is costly due to infrastructure requirement and a high opportunity cost (Konar et al. 2012; Yang et al. 2006; Aldaya et al. 2010). However, green water could be directly used in agriculture. Moreover, temperature change affects crop growth, development and yield, and grain quality especially the development rate as reported in the previous researches (e.g., Sarker et al. 2012; Luo 2011; Christensen et al. 2007). Negative effects of climate change on food and water security could also be partly associated with a significant and direct relationship between T and evapotranspiration (Xing et al. 2014; Peterson et al. 2002). In fact, a T increase might increase evapotranspiration and crop water demand. Under such circumstances, farmers cannot be allowed to fully irrigate their crops due to water shortage under climate change by applying deficit irrigation strategies. However, deficit irrigation (as a rational solution under water shortage) can lead to a significant reduction in crop yields due to a significant linear relation between crop yield and crop water use (Karandish 2016; Payero et al. 2006; Klocke et al. 2004; Stone 2003). Therefore, long-term climate data analysis particularly for rainfall and temperature, which provides valuable reference for future water resources and crop water requirements, is required to develop future strategies for efficient water and crop planning (Reddy et al. 2014). Assessing the related risks to extreme temperature and consequently, exploring adaptation solutions requires identifying the temperature thresholds. In fact, exploring the influences of high temperatures on crop yield in different growth stages may help with defining critical phenophases. Therefore, the investigations could be focused on these stages. Results of field investigations in which the negative effects of high temperature on crop yield are studied under different conditions could be helpful for improving crop models and consequently for quantifying the influence of temperature variations on crop yield at the regional scale (Luo 2011).

Analyzing and predicting the change in critical climatic variables is more essential in arid regions such as Iran where dry condition may increase under global warming if no adaptation solutions is undertaken. Under such circumstances, the process of desertification will be aggravated due to the growing influence of humans and domestic animals on fragile and unstable ecosystems (Goyal 2004). In Iran, land degradation in the past decades through overexploitation of water resources together with converting forest and rangelands to cultivated land and overuse of woodland plants as fuel led to a serious desertification risk (Tabari et al. 2011; Modarres and da Silva 2007; Ghahraman 2006; Raziei et al. 2005). Thus, achieving water and food security requires serious attempts to quantify the probable effects of climate change on meteorological and hydrological variables. Some researchers investigated the effects of climate change on climatic variables in different parts of Iran. Abbaspour et al. (2009) have assessed the impact of climate change on water resource components in Iran using Canadian Global Coupled Model (CGCM 3.1) for three scenarios of A1B, B1, and A2. Their results indicate that the wet regions of the country will receive more rainfall, while the dry regions will receive less. However, both monthly minimum and maximum temperature will increase under climate change. Tabari and Hosseinzadeh Talaee (2011) have investigated the annual and seasonal precipitation trends at 41 stations in Iran for the period 1966–2005 using three methods of Mann–Kendall, Sen's slope estimator and linear regression. The results indicated a decreasing trend in annual precipitation at about 60% of the stations which was significant at seven stations at the 5% significance level.

Although GCMs provide robust information regarding the quantitative effects of global warming, their coarse resolution is insufficient for analyzing local researches. Therefore, the projections of global changes should be downscaled when local variability of weather data under climate change is investigated. Downscaling methods are generally classified in two groups: statistical and dynamical methods. Detailed information on these methods can be found in the literature (Fowler et al. 2007; Wilby et al. 2004; Xu 1999; Hewitson and Crane 1996). Stochastic weather generator models are a kind of statistical downscaling methods by which long synthetic series of data are stochastically generated (Hashmi et al. 2011). When these models are used, missing data are also filled and different realizations of the same data are produced (Wilby 1999). In these methods, random numbers are employed and the observed time series of a station or a site are taken as input parameters (Hashmi et al. 2011).

The Long Ashton Research Station Weather Generator (LARS-WG) is a stochastic weather generator which was developed by Semenov and Barrow (2002). In the LARS-WG, the climate projections from 15 GCMs of IPCC AR4 are incorporated. This model can be employed for generating time series of precipitation, cardinal temperatures and radiation for both current and future climates (Ouyang et al. 2014). LARS-WG has been reported to provide reliable results for climate change studies in different parts of the world (Luo 2016; Agarwal et al. 2014; Hashmi et al. 2011). The high capability of this model to downscale weather data in arid regions such as Iran has also been

reported (Almasi and Soltani 2016; Kazemi-Rad and Mohammadi 2015; Osman et al. 2014; Etemadi et al. 2014, 2012; Chen et al. 2013; Dastorani and Poormohammadi 2012). Even for the driest regions of Iran, LARS-WG yielded reliable results (Goodarzi et al. 2015).

Although LARS-WG has been widely used for downscaling GCM data, literature reviews revealed that earlier studies have mainly focused on the downscaling of only one or two GCMs in a specific climatic region, while long-term changes in climatic variables in different climatic zones in Iran projected by different GCMs did not receive enough concern globally and locally. Different GCMs may yield different responses to the same external conditions and result in differences in their outputs (Fowler et al. 2007). Therefore, the outputs of a few GCMs could not be suitable for developing adaptation solutions to global warming. Assessment of climate change impact by a large ensemble of GCMs and analysis of the associated uncertainties are essential for estimating the potential consequences of anthropogenic climate change and preparing adaptation solutions. Policy makers and planners require such information for preparing adaptation and mitigation plans to reduce possible negative impact of climate change. This study aims to apply the outputs of all the GCMs incorporated in LARS-WG to investigate the possible effects of global warming on key weather variables and cereal production. Although new scenarios (Representative Concentration Pathway: RCP) have been recently developed, they have not yet been incorporated in LARS-WG. Hence, this study makes use of the outputs of the 15 GCMs used in the IPCC AR4 under the SRES scenarios incorporated in LARS-WG. The precipitation and temperature data for the historical and future periods from the 15 GCMs under three scenarios of A1B, A2 and B1 in five climatic zones of Iran (i.e., hyper-humid, Mediterranean, semi-Arid, arid and hyper-Arid) were analyzed. The analysis was carried out for the base period (1981–2010) and three future periods over the 21th century including 2011–2040 (early-century period), 2041–2070 (mid-century period) and 2071–2100 (late-century period). The uncertainties in GCMs and SRES scenarios for precipitation and temperature projections were also quantified. Finally, the possible influence of climate change on cereal production in the country was investigated in terms of crop water requirement, yield and water use efficiency.

2 Materials and methods

2.1 Study area and data collection

Iran lies between 25°00′N–38°39′N latitude and 44°00′E–63°25′E longitude and spans an area of 1,640,195 km². The

elevations range from −32 m below the sea level up to 5428 m with a national average of 1200 m. Based on de Martonne climate classification, there are five climatic regions in Iran including hyper-arid, semi-arid, arid, Mediterranean and hyper-humid with a general climate of arid and semi-arid (Tabari et al. 2014). For this study, 52 synoptic stations located in the five climatic zones were selected (Fig. 1) for which 30-year daily weather data including minimum (T_{min}) and maximum (T_{max}) temperature, precipitation (P) and radiation were collected for 1981-2010 (i.e., base period). Based on the available data, the long-term areal average of T_{min}, T_{max} and annual P are 12.4, 25.18 °C and 243.6 mm, respectively. The southeast (Sistan and Balouhestan province) and north (Gilan province) parts of the country receive the lowest (104.3 mm) and highest (1032.9 mm) annual P, respectively.

To obtain future climatic variables, the 15 GCMs used for the IPCC AR4 were selected because their data for the selected SRES scenarios are embedded in LARS-WG model. The models used in this research are listed in Table 1. Three emission scenarios including B1 (low emission of GHGs), A1B (medium emission of GHGs) and A2 (high emission of GHGs) were considered. These scenarios were selected because the qualitative results derived from them are mostly valid for the other SRES scenarios as well (IPCC 2007).

2.2 Downscaling weather data with LARS-WG

LARS-WG is a stochastic weather generator used to generate long-term daily weather data series at a single site
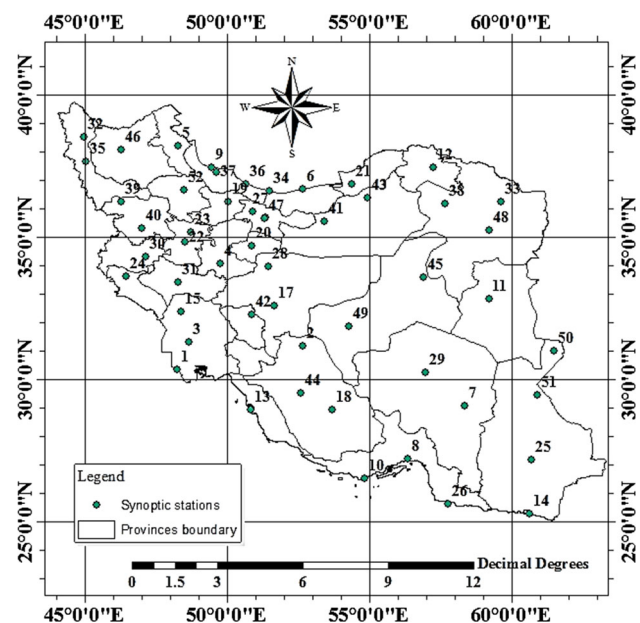

Fig. 1 Study area and the locations of 52 synoptic stations

Table 1 The global climate models used in this research (GCMs from IPCC AR4)

No.	Model	Scenarios			Research center	Country	Resolution
		A1B	A2	B1			
1	BCM2	✔		✔	Bjerknes Centre for Climate Research	Norway	1.9° × 1.9°
2	CGMR	✔			Canadian Center for Climate Modelling and Analysis	Canada	3.75° × 3.75°
3	CNCM3	✔	✔		Canadian Centre for Climate Modelling and Analysis	Canada	1.9° × 1.9°
4	CSMK3	✔		✔	Australia's Commonwealth Scientific and Industrial Research Organization	Australia	2.8° × 2.8°
5	FGOALS	✔		✔	Institute of Atmospheric Physics	China	2.8° × 2.8°
6	GFCM21	✔	✔	✔	Geophysical Fluid dynamic Laboratory	USA	2.5° × 2°
7	GIAOM	✔		✔	Goddard Institute for Space Studies	USA	3° × 4°
8	HadCM3	✔	✔	✔	UK Met. Office	UK	2.5° × 3.75°
9	HadGEM	✔	✔		UK Met. Office	UK	1.3° × 1.9°
10	INCM3	✔	✔	✔	Institute for Numerical Mathematic	Russia	4° × 5°
11	IPCM4	✔	✔	✔	Institute Pierre Simon Laplace	France	2.5° × 3.75°
12	MIHR	✔		✔	National Institute for Environmental Studies	Japan	2.8° × 2.8°
13	MPEH5	✔	✔	✔	Max-Planck-Institute for Meteorology	Germany	1.8° × 1.8°
14	NCCCSM	✔	✔	✔	National Centre for Atmospheric Research	USA	1.4° × 1.4°
15	NCPCM	✔	✔		National Center for Atmospheric Research	USA	2.8° × 2.8°

under both current and future conditions. LARS-WG uses observed daily weather data for a given site to compute a set of parameters for probability distributions of weather variables as well as correlations between them, which are used to generate synthetic weather time series of arbitrary length by randomly selecting values from the appropriate distributions. Semi-empirical probability distributions are used for P simulation and a normal distribution for temperature (T). Moreover, semi-empirical distributions with equal interval size are used for estimating solar radiation for a given set of parameters (Semenov and Barrow 2002).

In LARS-WG, there are three steps to generate synthetic weather data: model calibration, model validation and generating the synthetic weather data. SITE ANALYSIS function is used for the model calibration through which observed weather data are analyzed to determine their statistical characteristics. These information are stored in two parameter files for the other steps. The calibration process is based on the comparison of the statistical properties of the synthetic time series versus the observed data for each station (Agarwal et al. 2014). In this stage, the statistical properties (including monthly mean, standard deviation, 95% percentile of monthly P or T, t test and F-test) of the observed and simulated time series for each station are compared for the base period of 1981–2010. To validate LARS-WG, derived parameter files from the observed weather data during the calibration process are used to generate a 30-year long daily synthetic weather time series with the same statistical characteristics as the original observed data (Chen et al. 2013). Thereafter, the

statistical characteristics of the observed and synthetic weather data are compared to assess the ability of LARS-WG to simulate P, T_max, and T_min at the chosen sites in the study. Once LARS-WG has been calibrated using observed weather data for a given site and its performance has been verified, the parameter files derived from observed weather data during the model calibration process are used to generate synthetic weather data corresponding to a particular climate change scenario simulated by GCMs having the same statistical characteristics as the original observed data, but differing on a day-to-day basis (Chen et al. 2013; Agarwal et al. 2014). Synthetic data corresponding to a particular climate change scenario may also be generated by applying GCM-derived changes of precipitation, temperature and solar radiation to the LARS-WG parameter files.

To generate future climate scenarios for a station, LARS-WG baseline parameters calculated during the calibration process were adjusted by monthly Δ-change factors calculated from the differences between the future and baseline periods. These Δ-change factors were then applied as relative changes to LARS-WG parameters for the baseline P and T of each station in order to generate daily time series for the future periods. In this study, the climate scenarios based on the A1B, A2 and B1 scenarios simulated by the selected 15 GCMs (Table 1) were generated by using LARS-WG for the time periods of 2011–2040, 2041–2071, and 2071–2100 to predict the future change of precipitation and temperature in Iran. A detailed description of the different steps involved in LARS-WG for

downscaling climate change projections is given in Semenov and Stratonovitch (2010).

After downscaling weather data at 52 synoptic stations, mean daily and monthly values of the generated data for each time period were compared with the ones of the base period to explore the possible impact of climate change. To do so, the downscaled weather data at the stations located in each climatic zone were averaged (i.e., areal average) to represent the weather data over that zone. The averages over the country (national averages) were also calculated. The comparison was carried out for the annual and seasonal time-scales. In the seasonal scale, four seasons were defined based on the national standard of Iran: (i) spring: April, May and June (AMJ), (ii) summer: July, August and September (JAS), (iii) autumn: October, November and December (OND), and (iv) winter: January, February and March (JFM).

2.3 Mann–Kendall trend analysis

The rank-based nonparametric Mann–Kendall method (Mann 1945; Kendall 1975) was applied to the long-term data in this study to detect statistically significant trends. In this test, the null hypothesis (H_0) is that there has been no trend in P, T_{min} and T_{max} over time and the alternate hypothesis (H_1) is that there has been a trend (increasing or decreasing) over time. The mathematical equations for calculating the Mann–Kendall statistics S, $V(S)$ and standardized test Z statistics are as follows:

$$S = \sum_{i=1}^{n-1} \sum_{j=i+1}^{n} \text{sgn}(X_j - X_i), \tag{1}$$

$$\text{sgn}(X_j - X_i) = \begin{cases} +1 & \text{if } (X_j - X_i) > 0 \\ 0 & \text{if } (X_j - X_i) = 0 \\ -1 & \text{if } (X_j - X_i) < 0 \end{cases}, \tag{2}$$

$$V(S) = \frac{1}{18}[n(n-1)(2n+5)] - \sum_{p=1}^{q} t_p(t_p - 1)(2t_p + 5), \tag{3}$$

$$Z = \begin{cases} \dfrac{S-1}{\sqrt{VAR(S)}} & \text{if } S > 0 \\ 0 & \text{if } S = 0 \\ \dfrac{S+1}{\sqrt{VAR(S)}} & \text{if } S < 0 \end{cases}. \tag{4}$$

In these equations, X_i and X_j are the time series observations in chronological order, n is the length of time series, t_p is the number of ties for pth value, and q is the number of tied values. Positive Z values indicate an upward trend in the time series, while negative Z values indicate a negative trend. If $|Z| > Z_{1-\alpha/2}$, H_0 is rejected and a statistically significant trend exists in the time series. The critical value

of $Z_{1-\alpha/2}$ for a p-value of 0.05 (selected for this study) from the standard normal table is 1.96. The magnitude of the trends for the study variables for the period 1980–2010 was determined by the Sen's slope estimator. If a linear trend is present in a time series, then the true slope (change per unit time) can be estimated by using a simple nonparametric procedure developed by Sen (1968). The slope estimates of N pairs of data are first computed by:

$$Q_i = \frac{x_j - x_k}{j - k} \quad \text{for } i = 1, \dots, N, \tag{5}$$

where x_j and x_k are data values at times j and k ($j > k$), respectively. The median of these N values of Q_i is Sen's estimator of slope. The Sen's slope estimator is then computed based on N:

$$\begin{cases} \text{when } N \text{ is odd} & Q_{med} = Q_{\left[\frac{N+1}{2}\right]} \\ \text{when } N \text{ is odd} & Q_{med} = \frac{1}{2}\left(Q_{\left[\frac{N}{2}\right]} + Q_{\left[\frac{N+2}{2}\right]}\right) \end{cases}. \tag{6}$$

Finally, Q_{med} is tested with a two-sided test at the $100(1-\alpha)\%$ confidence interval and the true slope may be obtained by the nonparametric test (Partal and Kahya 2006).

2.4 GCMs and SRES scenarios uncertainty

A plausible range was quantified to illustrate the uncertainty in P, T_{min} and T_{max} projections in the various climatic zones of Iran. The change in the mean value of these variables for each future period (average of the 30 years for 2011–2040, 2041–2070 and 2071–2100) from the base period was determined for estimating the plausible range for both the annual and seasonal scales. Different probability distribution functions (PDFs) were fitted to the GCMs projections for each scenario and then, the Kolmogrov–Smirnov test was used to evaluate the goodness-of-fit of these functions. The Kolmogrov–Smirnov statistic (D) is determined based on the largest vertical difference between the theoretical and the empirical cumulative distribution function (CDF) as follows:

$$D = \max_{1 \le i \le n}\left[F(x_i) - \frac{i-1}{n}, \frac{i}{n} - F(x_i)\right]. \tag{7}$$

The 5% significant intervals were selected to analyze the hypothesis regarding the distribution form. Thereafter, the CDFs were computed based on the best fitted function for both the seasonal and annual changes in P, T_{min} and T_{max} in the future periods projected by GCMs under A1B, A2 and B1 scenarios compared to the base period. The uncertainty range was presented as the 5th and 95th percentile intervals from the CDFs.

2.5 Performance evaluation criteria

The statistical parameters including the percentage of difference between observed and generated data (DF) (Reddy et al. 2014), model efficiency (Ef) and root mean square error (RMSE) were considered for comparing the observed and simulated weather data as follows.

$$DF = \frac{(Y_i - X_i)}{X_i} \times 100 \tag{8}$$

$$Ef = \frac{\sum_{i=1}^{n}(X_i - \bar{X})^2 - \sum_{i=1}^{n}(Y_i - X_i)^2}{\sum_{i=1}^{n}(X_i - \bar{X})^2} \tag{9}$$

$$RMSE = \sqrt{\frac{\sum_{i=1}^{n}(X_i - Y_i)^2}{n}} \tag{10}$$

where X_i, Y_i, $\bar{X}$ and $\bar{Y}$ are respectively observed, simulated, average of observed and average of simulated data. N denotes the number of observed/simulated data. DF was used to calculate percentage change in the climate variables with respect to the base period. The lowest values of DF and RMSE and values near unity for Ef denote higher simulation accuracy.

3 Results and discussions

3.1 Evaluating LARS-WG outputs

For the base period (1981–2010), the percentage difference between the observed and simulated values of annual P, T_{min} and T_{max} is illustrated in Fig. 2. Precipitation is generally overestimated, with the highest bias in the southern and southeastern parts of Iran and the lowest one in the northern, northeastern and northwestern parts. However, T_{max} is underestimated in a small area, while T_{min} is generally overestimated. Comparison of the observed and LARS-WG simulated data reveals that the model performs better for non-monsoon months (June–September) when there is less rainy days and lower P amount (Fig. 3). The largest bias between the observed and generated data is observed in March–May period when the higher variability of P and T occurs. The model shows a higher ability for temperature simulation compared with precipitation. These results are in agreement with the findings of Reddy et al. (2014) and Agarwal et al. (2014) who found better results for simulating T than P when comparing the observed and generated data.

The model's validation results in terms of normalized root mean square error (NRMSE) (2.14–31.33, 0.14–0.38 and 0.17–0.54 for P, T_{min} and T_{max}, respectively) and Ef (near unity for all the considered variables) indicate that LARS-WG can generate the selected climatic variable

quite well (Table 2). However, monthly comparison between the observed and LARS-WG simulated P for the five climatic zones in Fig. 3 reveals that the model ranks first for simulating the climate variables in the Mediterranean and sub-humid climatic zones, while the higher variability of monthly P in the other climatic zones led to lower Ef and higher NRMSE. Overall, the statistical results are satisfactory for the five climatic zones since no significant difference is found between the observed and generated data based on t-test analysis (p-value < 0.05). These results are in accordance with the reported results in the previous precipitation- and temperature-related researches (Zhang et al. 2014; Hashmi et al. 2011).

3.2 Precipitation analysis

3.2.1 Historical precipitation trend

Figure 4 shows the results of trend analysis for annual and seasonal P, T_{min} and T_{max} during the base period. The results show that although there is a slight decrease in the average annual P over the country during 1981–2010, it is not significant according to the MK test. An insignificant annual P trend in most of the stations in Iran has also been reported by Tabari and Hosseinzadeh Talaee (2011), Raziei et al. (2005) and Modarres and da Silva (2007). The average of the Z values over different stations for P is equal to −0.3, indicating a slight decrease in annual P at the national level. Also, it can be observed that annual P in 19.4% of the stations is decreasing, although it is not significant. An increasing trend can be found at the remaining stations, of which only Bam, Khoy and Sanandaj stations have a statistically significant trend. Tabari and Hosseinzadeh Talaee (2011) reported that during 1966–2005, most of the stations located in Northern Iran had decreasing trends, while most of the stations located on the northern coasts of the Oman Sea and the Persian Gulf in the southern part of Iran had increasing trends of annual P.

For spring P, a significant decreasing trend is observed only at Tabass station (Fig. 4), while four stations (Hamedan, Khoramabad, Saghez and Zanjan) show a significant increase in spring P with Z > 1.96. The summer P for all stations shows insignificant change, with an insignificant decrease in 63.5% of the stations (Fig. 4). A general decrease is observed in autumn P with a significant trend in seven stations (Ghazvin, Gorgan, Hamedan, Kerman, Khoy, Sanandaj and Zanjan). Nevertheless, six stations (Bojnurd, Boushehr, Isfahan, Ghom, Ramsar and Tabass) experienced a slight but not significant increase in autumn P during 1981–2010. With the exception of a significant decrease in Bandar Abbas and Bandar Lengeh stations, no significant change in winter P is observed for the other stations. Generally, winter P decreased in 44% of
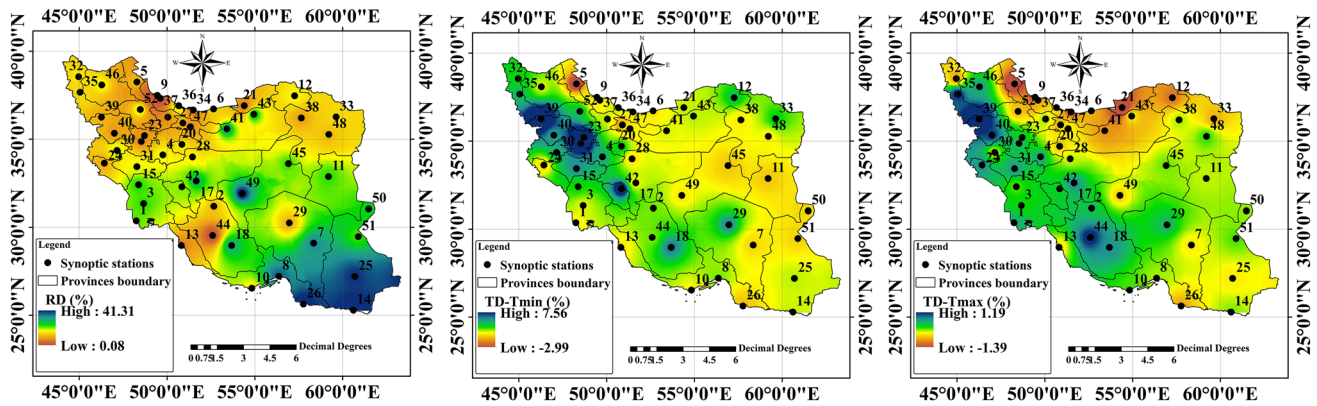
Fig. 2 Percentage difference between the observed and simulated (i.e., DF) P (*left*), T$_{min}$ (*middle*) and T$_{max}$ (*right*) during 1980–2010

the stations. This result is in agreement with some previous researches which reported a negative trend in winter P over the past decades (Nazemosadat et al. 2006; Tabari and Hosseinzadeh Talaee 2011).

3.2.2 Future precipitation change

Using the probability density functions (PDFs), the projection of precipitation for the 15 GCMs under the A1B scenario and also for the ensemble average of the GCMs under three SRES scenarios (i.e., A1B, A2 and B1) is calculated (not shown). The probability of P occurrence under a certain value is equal to the area under the curve to the left of that value. The total area under a PDF is equal to one. Results show both inter-annual variability (i.e., variation of an individual PDF) and probable uncertainty (i.e., differences between the PDFs of different GCMs). The hyper-humid regions have the highest inter-annual variability of P with more flat PDFs compared the other regions. However, the uncertainty is greater than inter-annual variability of P for the hyper-arid and arid regions.

A closer agreement is observed between GCMs PDFs (or scenario PDFs) with the extracted PDFs for the base period in the early periods compared with those for the later periods (not shown). In fact, in the early period, the inter-annual variability of P is higher than the difference between GCMs or scenario PDFs for all regions while it is opposite for the mid and late periods. The difference between the SRES scenarios well represents the uncertainty in P projections in the future periods in addition to the inter-annual variability of P. The difference between GCMs or scenario PDFs indicates different behaviors of the projected P for different GCMs and scenarios as can be seen for the later periods. Such different behaviors may be associated with the different resolutions of ocean models for different GCMs. In fact, better simulation of sea ice extent, sea surface temperature, surface heat, ocean heat

transfer process and momentum fluxes under an ocean model in GCMs considerably affect climate processes (CCSP 2008). The difference between GCMs could also be attributed to several factors such as the prognostic variable for cloud characterization and the compatibility between the heat and water budget of the atmospheric and ocean models (Randall et al. 2007). The projection differences between the three SRES scenarios are mainly due to the different assumptions related to economic, social and environmental modes.

The results of 35 ensembles (i.e., projections from 15 GCMs and three scenarios, Table 1) indicate that most ensembles show an increase in mean annual P and a few ensembles show a decrease. However, the average value yielded from 15 GCMs under the three scenarios as well as the median values for PDFs under the three scenarios of A1B, A2 and B1 indicate a general increase in annual P in the study area. Based on a physical law, any rise in T will increase the atmospheric water-holding capacity. In fact, the main reason which led to P increase is the increase in atmospheric water vapor content. Increased T in the study area is discussed in the following sections.

Based on the average results of the 15 GCMs for each scenario, the national average of annual P was calculated for the base and future periods and results are summarized in Table 3. Compared to the base period, climate change projections show a positive increase of the average annual precipitation at the national level under A1B, A2 and B2 scenarios with a range of 8.14–21.86%. Despite an overall increase in annual P in the country during 2011–2100, the share of regions which annually receive lower P than the national average will slightly increase by 1.5–3.3% compared with those for the base period (Table 3). The national average of annual P is 243.6 mm in the base period when 58.4% of the country receive less P than 243.6 mm. During 2011–2100, annual P increases by 8.14–21.86%. Nevertheless, 57.8–60.3% of the study area will receive less P
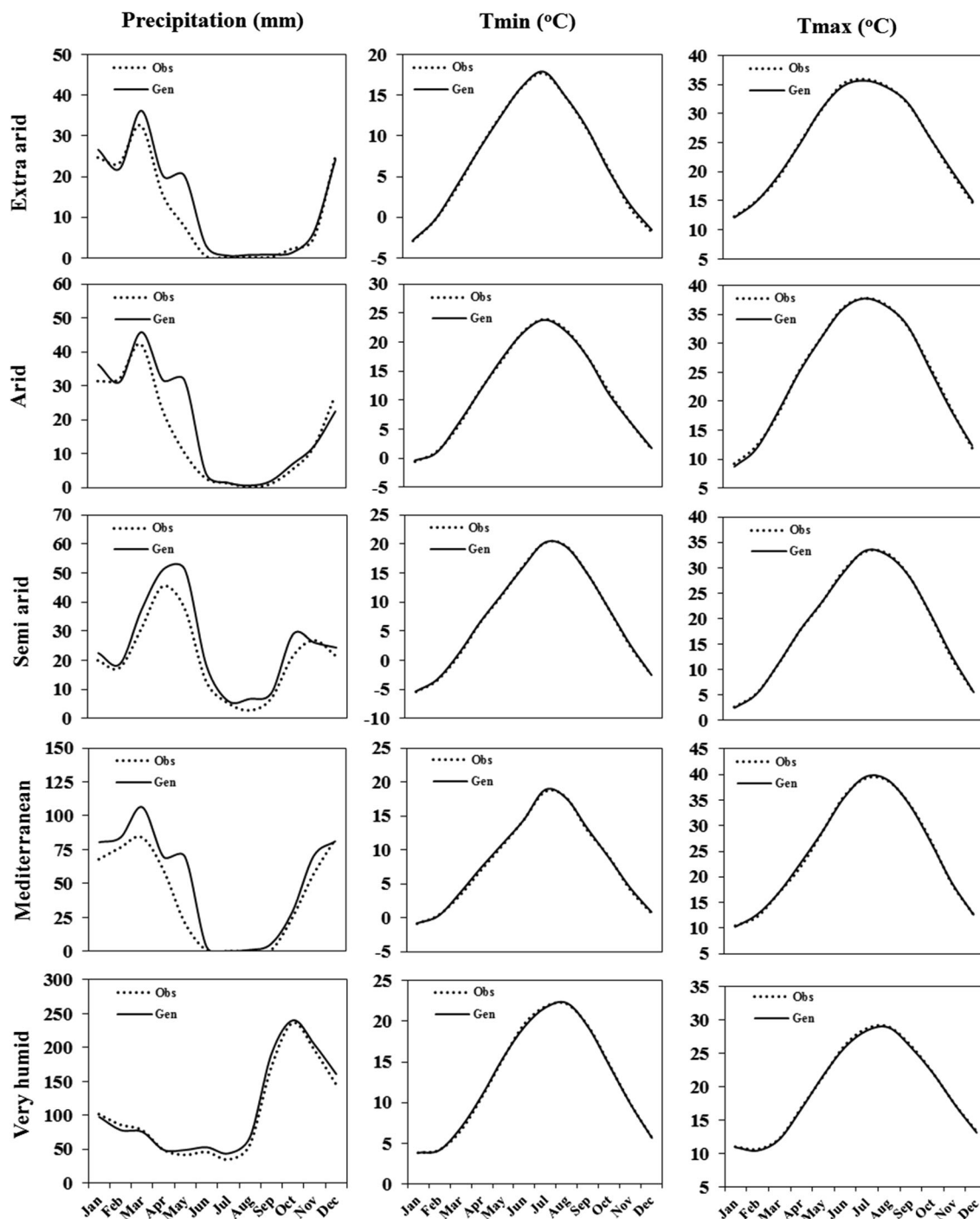
Fig. 3 Monthly variation of the observed and LARS-WG simulated climate variables for five climatic zones during 1981–2010

than the national average in the future periods. However, a slight increase in the share of regions with higher P than the national average is observed under the A2 and B1 scenarios during 2011–2040. Such results demonstrate a non-uniform spatial increase in P under projected climate change which is also obvious in Fig. 5.

Figure 5 shows that the highest P increase under climate change will happen on the coasts of the Caspian Sea, the

Oman Sea and the Persian Gulf, and in the northern hill-sides of the Alborz Mountains and the western hillsides of the Zagros Mountains. Inversely, the lowest impact of climate change is expected for the west and northwest of Iran. In addition, climate change is also projected to have a significant effect on P thresholds (Fig. 5). During the base period, P ranges between 53.1 and 1679.5 mm in the study area, while climate change increases the minimum

Table 2 Statistical properties for comparing observed and simulated weather data during 1980–2010

Climate	St. no	Station	P		Rank	T_{min}		Rank	T_{max}		Rank
			NRMSE	EF		NRMSE	EF		NRMSE	EF	
Hyper-arid	1	Abadan	33.87	89.87	30	0.90	99.95	3	0.62	99.96	2
	7	Bam	50.53	71.76	45	1.47	99.90	8	0.86	99.91	7
	10	Bandar Lengeh	36.41	90.01	27	0.78	99.92	6	0.80	99.81	16
	14	Chahbahar	70.38	55.99	52	0.85	99.83	14	0.57	99.74	19
	17	Esfahan	46.36	72.97	44	2.40	99.93	5	1.45	99.89	9
	25	Iranshahr	54.92	60.83	51	0.74	99.97	1	0.86	99.89	9
	26	Jask	75.21	61.10	50	0.92	99.78	16	0.91	99.51	20
	28	Kashan	40.38	77.95	40	1.70	99.95	3	1.24	99.91	7
	29	Kerman	18.71	96.78	6	3.08	99.91	7	0.98	99.92	6
	45	Tabass	39.93	85.77	37	1.47	99.94	4	0.92	99.94	4
	49	Yazd	64.30	65.58	47	1.41	99.96	2	0.99	99.93	5
	50	Zabol	42.63	88.18	33	1.44	99.95	3	1.15	99.88	10
	51	Zahedan	45.33	76.24	42	2.32	99.88	10	0.88	99.92	6
Arid	2	Abadeh	24.15	93.77	17	3.83	99.89	9	1.05	99.94	4
	3	Ahwaz	33.06	90.78	26	0.86	99.96	2	0.64	99.96	2
	8	Bandar Abass	71.50	65.56	48	1	99.90	8	0.65	99.87	11
	11	Birjand	30.55	92.05	21	2.92	99.91	7	1.44	99.85	13
	13	Bushehr	17.02	98.41	1	0.84	99.94	4	0.80	99.90	8
	16	Doushan Tappeh	17.64	94.97	10	1.81	99.93	5	1.15	99.93	5
	20	Ghom	24.15	91.52	23	3.09	99.87	11	1.54	99.86	12
	38	Sabzevar	22.96	93.98	16	2.11	99.92	6	1.34	99.90	8
	41	Semnan	45.66	61.68	49	1.56	99.96	2	1.28	99.92	6
Semi-arid	4	Arak	21.90	92.03	22	3.92	99.90	8	2.03	99.86	12
	5	Ardebil	18.81	87.14	35	8.97	99.87	11	2.31	99.82	15
	12	Bojnurd	67.22	84.93	38	3.87	99.88	10	2.03	99.83	14
	15	Dezful	32.32	91.32	24	1.57	99.90	8	0.64	99.96	2
	18	Fassa	60.42	77.26	41	3.07	99.82	15	1.38	99.83	14
	19	Ghazvin	17.14	94.61	12	2.81	99.94	4	1.23	99.94	4
	22	Hamedan Foroudgah	14.50	96.13	8	8.27	99.85	13	1.34	99.95	3
	23	Hamedan Nozheh	12.76	96.65	7	14.58	99.78	16	1.21	99.96	2
	27	Karaj	16.84	95.10	9	3.25	99.86	12	1.56	99.90	8
	30	Kermanshah	26.82	89.43	31	2.96	99.92	6	1.16	99.94	4
	32	Khoy	21.36	86.31	36	2.73	99.96	2	2.16	99.86	12
	33	Mashhad	23.02	93.22	18	2.50	99.93	5	1.15	99.94	4
	35	Oroomieh	20.32	89.97	29	3.94	99.93	5	2.36	99.83	14
	43	Shahroud	42.22	67.08	46	2.51	99.92	6	1.24	99.94	4
	44	Shiraz	16.93	97.95	2	2.01	99.92	6	1.44	99.85	13
	46	Tabriz	20.99	88.99	32	2.11	99.97	1	1.11	99.97	1
	47	Tehran Mehrabad	19.14	94.38	14	1.95	99.92	6	1	99.95	3
	48	Torbate Heydarie	30.11	89.98	28	3.15	99.92	6	1.37	99.92	6
	52	Zanjan	32.54	73.63	43	4.82	99.93	5	1.97	99.89	9
Mediterranean	21	Gorgan	13.21	87.30	34	1.05	99.97	1	1.71	99.75	18
	24	Ilam	22.16	94.29	15	1.88	99.94	4	1.09	99.94	4
	31	Khoramabad	23.94	92.56	20	3.15	99.86	12	1.26	99.92	6
	39	Saghez	12.24	97.26	5	12.31	99.73	18	2.92	99.77	17
	40	Sanandaj	18.61	94.58	13	4.69	99.88	10	1.23	99.94	4
	42	Shahre Kord	28.51	90.98	25	12.06	99.75	17	0.87	99.97	1

Table 2 continued

Climate	St. no	Station	P		Rank	T_{min}		Rank	T_{max}		Rank
			NRMSE	EF		NRMSE	EF		NRMSE	EF	
Hyper-humid	6	Babolsar	17.48	93.08	19	1.02	99.96	2	1.01	99.91	7
	9	Bandar Anzali	10.99	97.46	4	1.26	99.94	4	1.61	99.83	14
	34	Noushahr	9.45	97.93	3	1.43	99.93	5	1.23	99.88	10
	36	Ramsar	32.44	78.83	39	1.29	99.94	4	0.70	99.96	2
	37	Rasht	12.45	94.62	11	1.29	99.95	3	1.26	99.88	10

NRMSE Normalized Root Mean Square Error, *EF* Model efficince
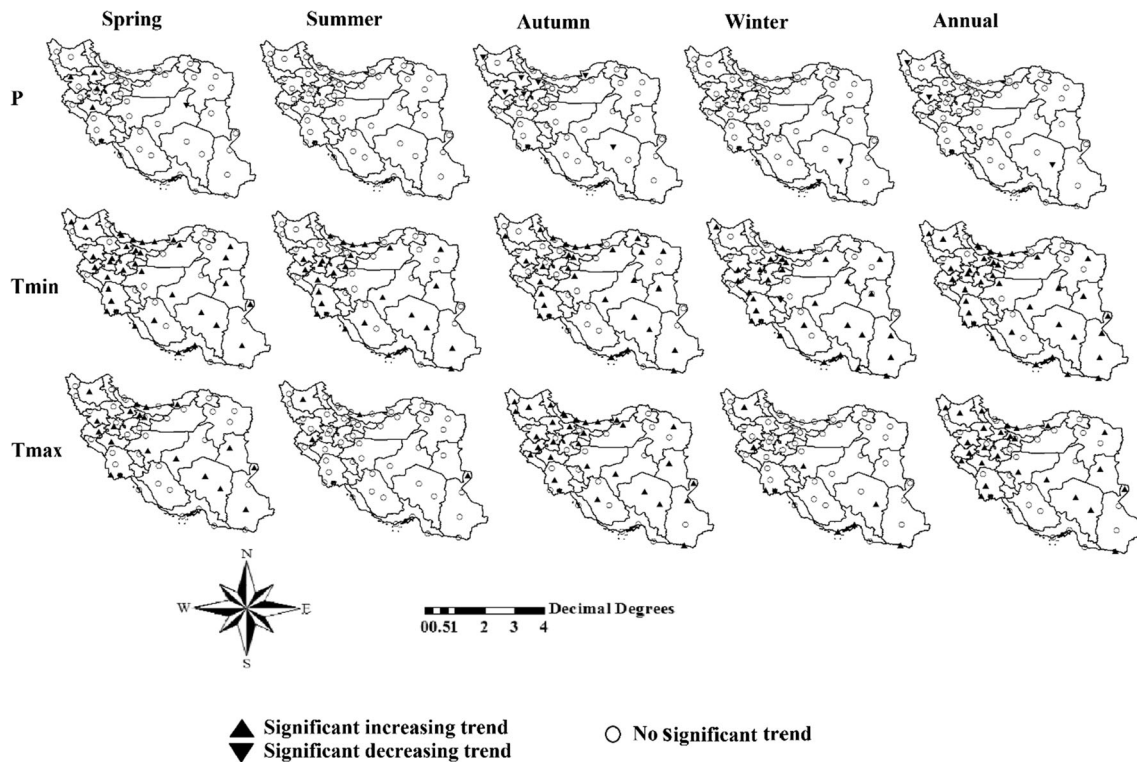

Fig. 4 Stations with increasing, decreasing and no trend at the 5% significance level for the annual and monthly P time series

threshold of P by 24.5% (i.e., under B1 scenario in 2071–2100) up to 35.84% (i.e., under A2 scenario in 2011–2040) and increases the maximum threshold by 0.3% (i.e., under A1B scenario in 2071–2100) up to 6.7% (i.e., under A2 scenario in 2011–2040).

The maps in Fig. 5 reveal that in the case of downscaled future P, each part of the country shows their own style of projection. Thus, the ensemble effects of the 15 GCMs on P were calculated for the five climatic zones and results are summarized in Table 4. Climate change projections show a P increase in all the climatic zones; however, some GCMs project a P reduction mainly in the Mediterranean and hyper-humid regions. The highest P increase corresponds to the hyper-arid and arid regions in which P increases by 27.9% under B1 scenario during 2071-2100 up to 83.3%

under A2 scenario in 2011–2040. The lowest increase occurs in the Mediterranean and hyper-humid climatic regions where P will increase by 1.98% under A1B scenario during 2071–2100 up to 9.5% under A2 scenario during 2011–2040. Dissimilar patterns of future P may be due to the local characteristics influencing P. A 15° difference in geographical latitude between the northern and southern parts of Iran, the existence of many folds, peaks and valleys and a combination of different fronts which initiate from different lands would cause different sources of P in Iran. In addition, being on the bank side of the Oman Sea and the Persian Gulf and the influence of the Mediterranean Sea in one hand, and the existence of Arabian and African arid deserts in the southwestern parts and Siberian wide plains in the northeastern part on the other

Table 3 Annual P increase and it's thresholds at the national level based on the average results of the 15 GCMs for each scenario in the future periods

Base	Scenario	Min (mm)	Max (mm)	Mean (mm)	SD (mm)	RPH (%)	RPL (%)	RPD (%)	RPD (%)	PI (%)
1980–2010	–	53.09	1679.52	240.26	153.98	41.65	58.35	–	–	–
2011–2040	A1B	67.12	1759.64	274.39	160.81	40.74	59.26	0	100	14.21
	A2	72.12	1791.62	292.78	172.42	42.11	57.89	0	100	21.86
	B1	67.11	1706.65	273.39	160.33	42.21	57.79	0	100	13.79
2041–2070	A1B	68.07	1726.43	264.85	152.32	40.62	59.38	4.34	95.66	10.23
	A2	68.13	1780.33	283.63	166.81	39.71	60.29	1.15	98.85	18.05
	B1	68.12	1724.02	271.43	157.14	39.82	60.18	0.21	99.79	12.97
2071–2100	A1B	68.12	1684.97	260.14	150.27	40.24	59.76	10.64	89.36	8.27
	A2	68.12	1699.14	273.68	163.00	39.83	60.17	10.09	89.91	13.91
	B1	66.11	1678.32	259.82	152.66	40.77	59.23	4.42	95.58	8.14

RPH regions with P higher than national average, *RPL* regions with P lower than national average, *RPD* regions with P decrease under climate change, *RPI* regions with P increase under climate change, *PI* increase in P

hand, would lead to different sources of P in Iran (Alizade et al. 2010). In fact, P in the northern and southern parts of the country comes from Monsoon and Siberian cold fronts and Mediterranean fronts respectively, while the central and eastern parts do not receive high P and stay as deserts and arid regions since they are located in the back of the Alborz and Zagros Mountains (Azarakhshi et al. 2013). This makes complicated the climate change effect study on the spatial distribution of P in Iran. Non-uniform spatial increase in P may threaten rainfed agriculture since green water is the main source for supplying crop water requirement. Under such circumstances, sustainable agriculture requires essentially prioritizing rainfed crop cultivation considering regional available green water under climate change. This need is more obvious when one considers that average annual P during 2041–2070 and 2071–2100 is less than that during 2011–2040 for the whole country as well as for the selected climatic zones (Table 4).

The seasonal pattern of P variations also represents a non-uniform temporal projected effect of climate change scenarios on P (Fig. 6). Despite a general P increase, the increase in autumn and winter periods (wet seasons) is higher than that for spring and summer periods (dry seasons) which may decrease the green water availability during the growing seasons. Increased P in wet seasons will lead to water-logging problems which requires installing costly drainage systems to relieve the further problems. On the other hands, increased P in dry seasons could provide favorable condition for weeds and pests growth and soil erosion through changing soil available water (Enete and Amusa 2010). These will have negative effects on crop growth and economic yield which in turn threaten the food security in the future.

Figure 6 shows that spring (10.2–23.18% increase in P), summer (58–65.4% increase in P) and autumn (640–674% increase in P) monsoons are expected to become wetter in the arid regions while winter P has the highest increase in the hype-arid regions accounted for 41–50.6%. During 2011–2100, the lowest change in autumn and winter P is observed in the hyper-humid regions where autumn P has a negative change during 2041–2100 (−2.2 to −10.64% decrease in P) compared to the base period (1981–2010). A negative trend is also observed in spring P of the Mediterranean climatic region (−2.7 to −7%) during 2041–2100 and in the semi-arid regions (−3.5%) during 2071–2100. In addition, summer monsoon precipitation likely decrease in both the semi-arid and Mediterranean climatic regions by −6.3 to −7.5% during 2071–2100. Since the influencing variables on climate could trigger abrupt transitions, P might decrease under a drier monsoon or increase under a more wet monsoon (Zickfeld et al. 2005).

To evaluate the probability of seasonal P variations, the range of seasonal uncertainty arising from the differences in the projections of different GCMs under the three SRES scenarios was estimated within the central 5–95% value of CDFs (i.e., CDFs represents the changes in seasonal P during the future periods relative to the base period). Figure 7 shows the range of seasonal P uncertainty for different climatic zones. No uniformity is observed in seasonal P changes as well as the annual one; rather they change from negative to positive for the future periods. Due to the complexity in interpreting P projections, not uniform pattern is observed in P changes during any season. Girvetz et al. (2009) has reported that different GCMs may not agree on whether P will increase or decrease even at a specific place and agree even less on the magnitude of the P change.
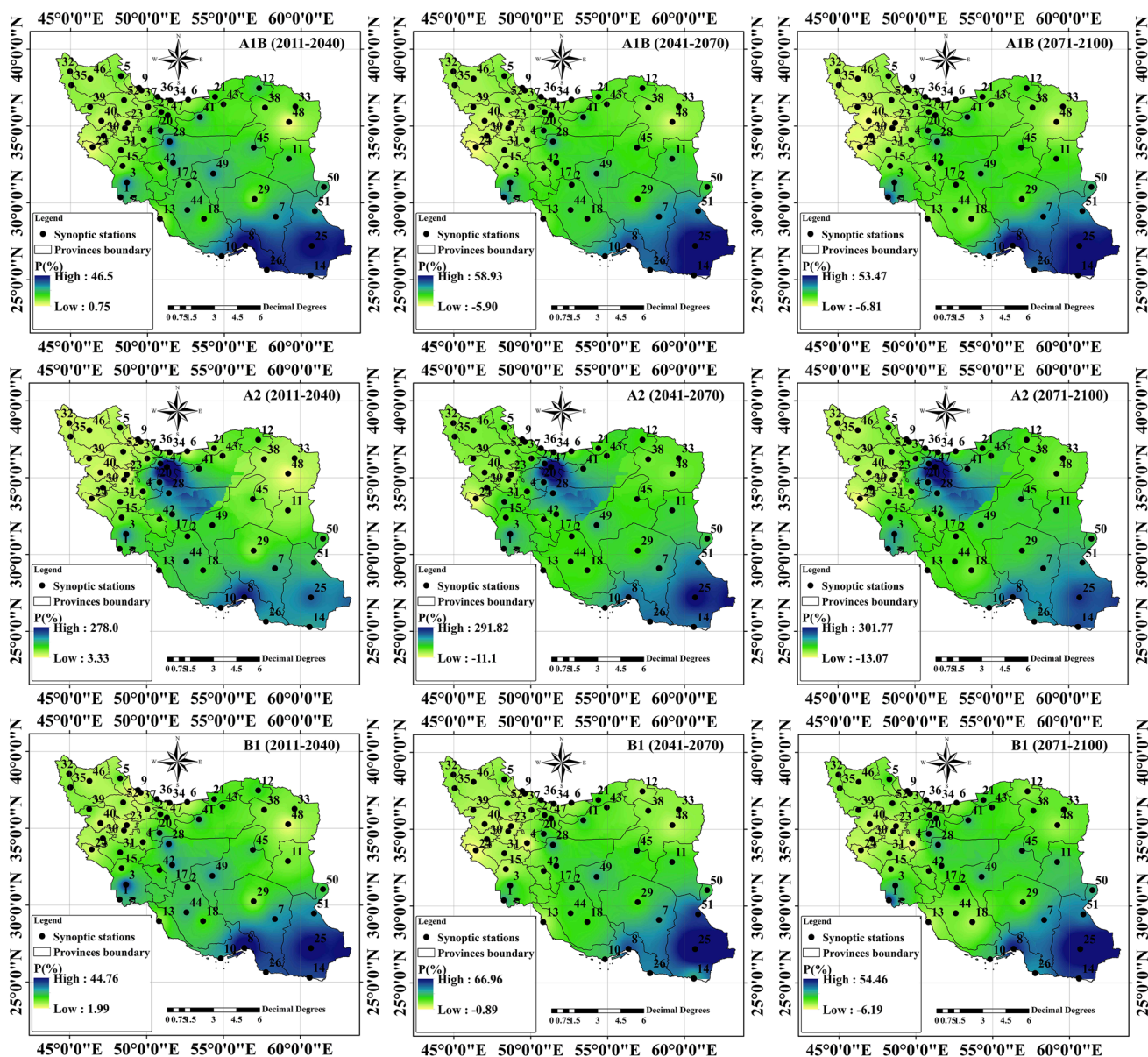
Fig. 5 Difference between P values for the base and future periods (as the ensemble average of the 15 GCMs) under different climate change scenarios up to 2100

Uncertainty decreases for all seasons in the different climatic zones in the mid- and late-century except for the winter season in the hyper-humid and arid climatic zones and the spring season in the other regions for which uncertainty decreases with time progress. Increase of uncertainty with time might be due to the uncertainties in climate sensitivity and the carbon cycle (Knutti et al. 2003). Similar results were reported by Minville et al. (2008) and Chen et al. (2011) for GCMs and GHGs. Regardless of the climatic zones, the highest range of uncertainty is projected in the rainy seasons of autumn and winter, while the lowest one is projected in the summer season which receives the lowest P during a year. Exception is for the hyper-humid regions in which the lowest

uncertainty corresponds to spring P. The larger uncertainty in rainy seasons was also reported by Agarwal et al. (2014). Figure 7 shows that seasonal P in the hyper-humid regions, which contributes a large part of the national P, has also the highest uncertainty, while the hyper-arid regions has the lowest uncertainty for seasonal P.

3.3 Temperature analysis

3.3.1 Historical temperature trend

The analysis of historical temperature trends shows an increasing trend in the annual average T_{min} and T_{max} time

Table 4 Climate change effects on annual P in the five climatic zone (i.e., as the ensemble average of the 15 GCMs for each scenario)

| Period	Climatic zone	P (mm)									
		Base	A1B			A2			B1		
			Mean	Min	Max	Mean	Min	Max	Mean	Min	Max
2011–2040	Hyper-arid	103.53	137.72	116.87	176.97	141.63	114.58	181.88	134.68	112.72	178.05
	Arid	187.68	227.35	196.91	271.43	344.00	311.06	384.83	227.03	192.88	266.53
	Semi-arid	288.68	323.06	293.36	348.36	333.26	300.22	363.13	320.16	294.46	347.30
	Mediterranean	457.81	503.38	459.43	593.03	509.83	453.04	603.35	513.74	468.21	589.38
	Hyper-humid	1254.49	1363.01	1231.99	1461.98	1373.14	1279.86	1499.26	1338.96	1264.69	1433.29
2041–2070	Hyper-arid	103.53	138.11	113.69	168.48	141.87	117.81	178.75	137.25	117.47	163.97
	Arid	187.68	219.42	187.80	250.69	338.27	298.46	373.31	222.41	193.14	258.46
	Semi-arid	288.68	307.73	279.82	344.44	317.75	289.65	363.19	317.45	292.38	343.54
	Mediterranean	457.81	475.14	427.73	532.30	496.11	431.6	560.84	497.56	446.84	550.17
	Hyper-humid	1254.49	1315.02	1195.87	1428.42	1344.91	1186.84	1449.41	1342.14	1215.35	1473.23
2041–2070	Hyper-arid	103.53	137.46	118.07	171.27	137.08	118.88	173.55	132.42	110.78	165.11
	Arid	187.68	219.44	178.09	258.28	338.86	304.07	385.92	216.42	175.77	243.71
	Semi-arid	288.68	299.53	276.16	326.04	303.14	277.64	334.17	302.95	273.52	333.80
	Mediterranean	457.81	466.90	414.29	519.75	467.55	418.78	525.75	480.33	439.02	543.35
	Hyper-humid	1254.49	1305.81	1203.15	1432.82	1317.61	1235.12	1443.42	1295.08	1167.62	1417.73
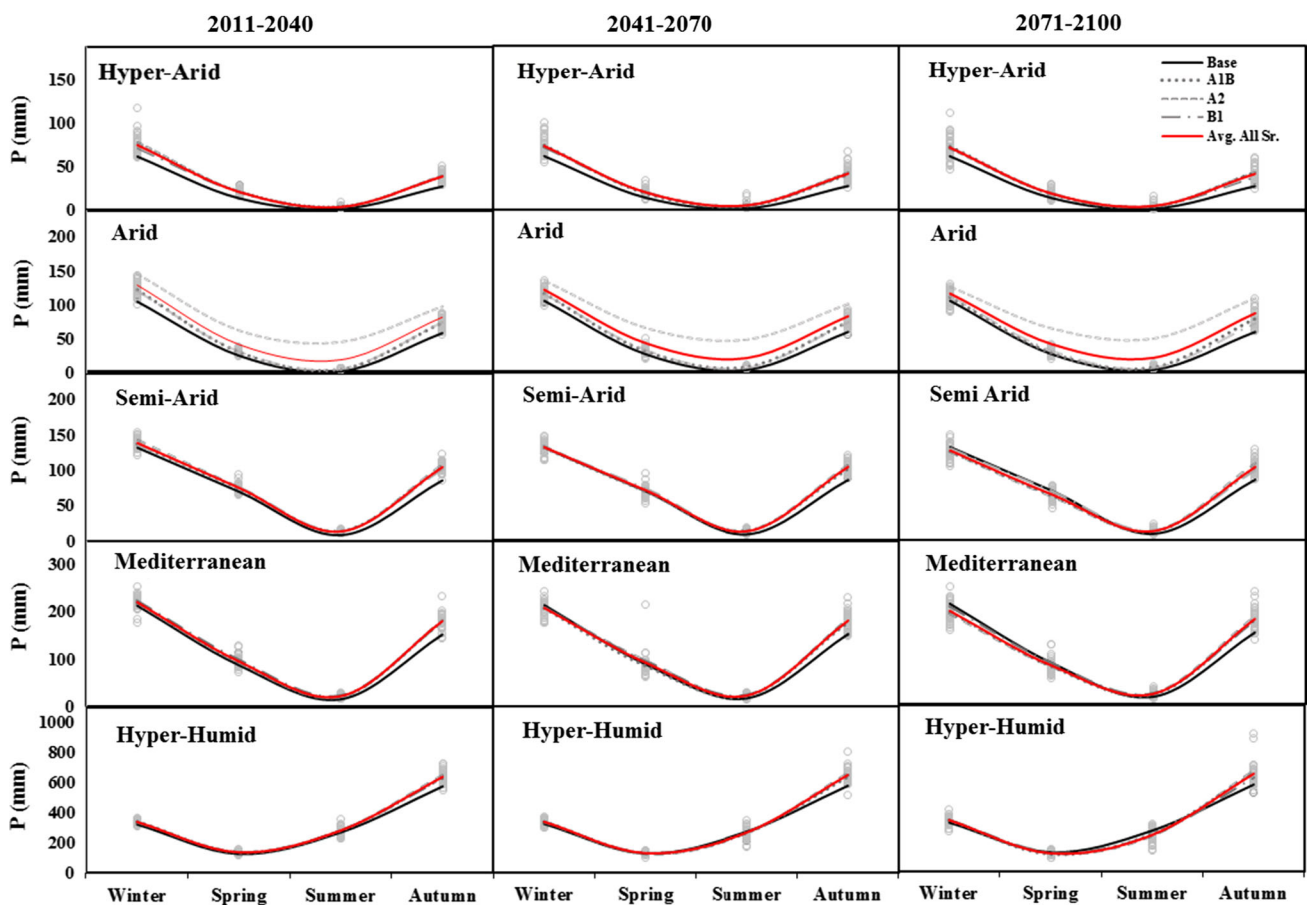
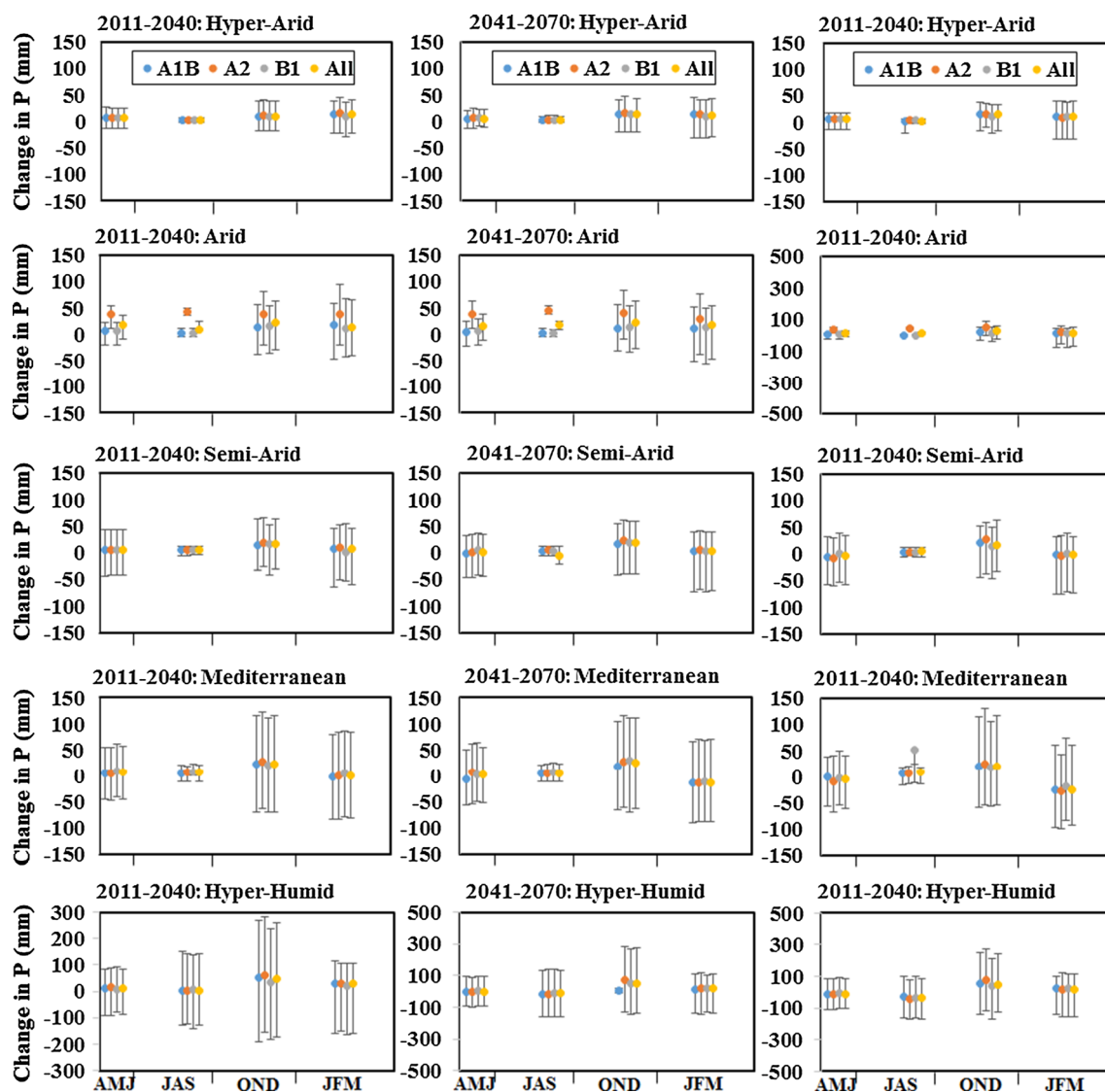**Fig. 6** Seasonal variation of P in different climatic zones under changing climate

Fig. 7 Range of change in seasonal P under different scenarios in different climatic zones of Iran (*lower* and *upper* ends indicate respectively the 5 and 95% intervals of the uncertainty range and *dot* shows the 50% value)

series (Fig. 4). T_{min} increased at the rate of 0.035–1.21 °C per decade during 1981–2010 with the minimum increase for Ghazvin station and the maximum one for Mashhad station, located in the semi-arid climatic zone. Totally, the lowest increase in T_{min} occurred in the Mediterranean climate followed by the semi-arid one. A slight reduction in T_{min} (i.e., 0.04–0.83 °C per decade) occurred in less than 22% of the stations during 1981–2010. For over 94% of the stations, an increase of 0.02–0.95 °C per decade is observed in the annual T_{max} series with the lowest and highest increases in the hyper-arid and semi-arid climatic zones, respectively (Tables 5, 6). Overall, the annual T_{min} and T_{max} trends are significant at 28.2 and 51.9% of the stations, respectively (Table 2; Fig. 4). The results generally indicate an overall warming climate in Iran, as reported by other researches (Abbaspour et al. 2009;

Dastorani and Poormohammadi 2012; Kazemi-Rad and Mohammadi 2015). Z statistics for seasonal average T_{min} and T_{max} show an obvious increase for all seasons for over 80% of the stations. This increase is significant in 53.8–63.9% of the stations in different seasons for T_{min}. A slight but not significant decrease in seasonal T_{min} is observed in five stations (Esfahan, Fassa, Ilam, Saghez and Shahrekord). T_{max} for 7.7–61.5% of the stations is found to have a significant increasing trend in spring, summer and winter, while about half of the stations in autumn experience a significant T_{max} increase.

3.3.2 Future temperature change

The PDFs for the projection of T_{min} and T_{max} for all GCMs under the A1B scenario and for the ensemble projections of

the 15 GCMs under three SRES scenarios (i.e., A1B, A2 and B1) show both inter-annual variability and probable uncertainty (not shown). Despite the negative change in both T_{min} and T_{max} under a few GCMs, the median values for PDFs under the three scenarios indicates a general increase in annual T_{min} and T_{max} in the study area. Same as P, a closer agreement between GCMs or scenarios PDFs with those for the base period is found in the early future periods compared to the later one (not shown). Based on the average results of the 15 GCMs for each scenario, the national average of annual T_{min} and T_{max} was calculated for the base and future periods and results are summarized in Table 5. A 7.1% (under A1B scenario during 2011–2040) up to 30.5% (under A2 scenario during 2071–2100) increase in national average of T_{min} can be found for the future periods with an ensemble average of 19.2% during 2011–2100. Taking the median of the 15 GCMs, the 90-year average increase (i.e., across 2011–2100) in T_{min} is around 17.4, 25.4 and 14.8% for the A1B, A2 and B1 scenarios, respectively.

Table 5 also shows a considerable increase in annual T_{max} in the future, accounted for 2.14–11.99% with an ensemble average of 6.16% during 2011–2100. However, the increase in T_{max} is lower than that for T_{min}. For 2011–2040, the A2 scenario projects the highest increase in T_{max}

with a 30-year average of 11.99%, while for 2041–2100, the highest increase in T_{max} corresponds to the A1B scenario with a 60-year average of 8.83%. The lowest increase in T_{max} is projected by the B1 scenario. Both T_{min} and T_{max} increases under climate change in the study area are supported by the results of the previous researches (Abbaspour et al. 2009; Dastorani and Poormohammadi 2012; Kazemi-Rad and Mohammadi 2015).

The spatial maps of the difference (%) in the T_{min} and T_{max} of the base and those for the future periods (i.e., based on the median of the 15 GCMs for three scenarios) indicate a general increase in both T_{min} and T_{max} in Iran except for a few parts of the country during 2011–2100 (Figs. 9, 10). The highest increase in both T_{min} and T_{max} occurs in the northwest part where the general climate is semi-arid. Similar to precipitation, climate change is also projected to have a significant effect on T_{min} and T_{max} thresholds (Figs. 8, 9). During the base period, the ranges of variation for T_{min} and T_{max} are 2.68–24.46 and 15.01–34 °C, respectively. Climate change is expected to increase the minimum threshold of T_{min} and T_{max} by 12.3–123.9 and 6.7–20%, respectively. The maximum threshold of T_{min} and T_{max} also increases by 1.6–10.2 and 2.9–8.8%, respectively.

Table 5 Annual T_{min} and T_{max} increase and thresholds at the national level based on the average results of the 15 GCMs for each scenario in the future periods

	Base	Scenario	Min (mm)	Max (mm)	Mean (mm)	SD (mm)	RTH (%)	RTL (%)	RTD (%)	RTD (%)	TI (%)
T_{min}	1980–2010	–	2.68	24.46	11.34	4.32	43.25	56.75	–	–	–
	2011–2040	A1B	3.45	25.03	12.14	4.30	43.29	56.71	0	100	7.05
		A2	4.00	24.96	14.42	4.16	42.82	57.18	0.30	99.70	27.16
		B1	3.01	24.87	12.25	4.22	42.55	57.45	0.10	99.90	8.02
	2041–2070	A1B	4.01	25.96	13.42	4.20	42.46	57.54	0	100	18.34
		A2	5.00	25.96	13.46	4.17	42.90	57.10	0	100	18.69
		B1	4.00	25.96	13.06	4.22	43.55	56.45	0	100	15.17
	2071–2100	A1B	5.01	26.96	14.37	4.24	42.66	57.34	0	100	26.72
		A2	6.00	26.96	14.76	4.17	43.94	56.06	0	100	30.16
		B1	5.00	25.96	13.76	4.24	44.27	55.73	0	100	21.34
T_{max}	1980–2010	–	15.01	34.00	25.19	3.83	48.87	51.87	–	–	–
	2011–2040	A1B	16.01	35.00	25.76	3.95	49.59	50.41	0	100	2.26
		A2	18.01	37.00	28.21	3.78	50.00	50.00	0	100	11.99
		B1	16.01	35.00	25.73	3.92	49.43	50.47	0	100	2.14
	2041–2070	A1B	17.00	35.92	26.92	3.86	49.48	50.52	0	100	6.87
		A2	17.01	35.93	26.87	3.86	49.41	50.59	0	100	6.67
		B1	16.01	35.00	26.31	3.82	49.49	50.51	0	100	4.45
	2071–2100	A1B	18.01	37.00	27.91	3.90	50.41	49.59	0	100	10.80
		A2	16.01	35.00	25.79	3.89	49.45	50.55	0	100	2.38
		B1	17.01	36.00	27.17	3.81	49.85	50.15	0	100	7.86

RTH regions with T higher than national average, *RTL* regions with T lower than national average, *RTD* regions with T decrease under climate change, *RTI* regions with T increase under climate change, *TI* increase in T (i.e., T refers to T_{min} or T_{max})

Table 6 Climate change effects on annual T_{min} and T_{max} in the five-climatic zone (i.e., as the ensemble average of the 15-models for each scenario)

Parameter	Period	Climatic zone	T (°C)									
			Base	A1B			A2			B1		
				Mean	Min	Max	Mean	Min	Max	Mean	Min	Max
T_{min}	2011–2040	Hyper-arid	16.03	16.78	16.70	16.87	16.78	16.69	16.86	16.70	16.63	16.79
		Arid	13.93	14.40	14.26	14.50	14.29	14.16	14.40	14.34	14.21	14.43
		Semi-arid	7.54	8.26	8.20	8.40	8.34	8.28	8.48	8.14	8.07	8.28
		Mediterranean	7.12	8.06	7.88	8.23	7.92	7.74	8.05	8.01	7.86	8.16
		Hyper-humid	13.20	13.71	13.65	13.87	13.81	13.74	13.96	13.71	13.64	13.86
	2041–2070	Hyper-arid	16.03	17.90	16.76	18.21	17.85	16.79	18.15	17.45	16.71	17.67
		Arid	13.93	15.50	14.37	15.83	15.31	14.24	15.62	15.05	14.30	15.30
		Semi-arid	7.54	9.37	8.23	9.71	9.40	8.32	9.73	8.84	8.13	9.09
		Mediterranean	7.12	9.20	7.96	9.59	8.98	7.85	9.33	8.74	7.92	9.04
		Hyper-humid	13.20	14.68	13.69	15.00	14.72	13.78	15.03	14.31	13.69	14.56
	2041–2070	Hyper-arid	16.03	18.83	18.10	19.20	19.15	18.02	19.68	18.04	17.55	18.32
		Arid	13.93	16.40	15.68	16.76	16.57	15.48	17.09	15.66	15.16	15.95
		Semi-arid	7.54	10.26	9.54	10.64	10.67	9.57	11.22	9.41	8.92	9.71
		Mediterranean	7.12	10.12	9.36	10.56	10.29	9.11	10.88	9.35	8.82	9.69
		Hyper-humid	13.20	15.44	14.79	15.80	15.80	14.80	16.29	14.81	14.37	15.12
T_{max} (°C)	2011-2040	Hyper-arid	29.04	29.45	29.34	29.60	29.45	29.34	29.60	29.39	29.29	29.54
		Arid	26.72	27.22	27.10	27.35	27.13	27.02	27.26	27.19	27.08	27.32
		Semi-arid	21.37	21.98	21.89	22.07	22.06	21.97	22.14	21.75	21.68	21.83
		Mediterranean	21.93	22.51	22.33	22.77	22.16	22.01	22.41	22.47	22.35	22.74
		Hyper-humid	20.04	20.43	20.34	20.59	20.52	20.44	20.65	20.44	20.34	20.59
	2041–2070	Hyper-arid	29.04	30.59	29.42	30.97	30.55	29.44	30.91	30.13	29.36	30.41
		Arid	26.72	28.36	27.19	28.71	28.20	27.08	28.54	27.92	27.15	28.19
		Semi-arid	21.37	23.16	21.99	23.47	23.15	22.05	23.44	22.47	21.75	22.69
		Mediterranean	21.93	23.73	22.44	24.23	23.27	22.05	23.73	23.24	22.39	23.66
		Hyper-humid	20.04	21.44	20.41	21.80	21.46	20.52	21.78	21.07	20.39	21.34
	2041–2070	Hyper-arid	29.04	31.56	30.76	32.00	31.87	30.68	32.48	30.77	30.21	31.14
		Arid	26.72	29.32	28.54	29.74	29.51	28.36	30.08	28.59	28.04	28.92
		Semi-arid	21.37	24.12	23.36	24.50	24.48	23.33	25.02	23.13	22.58	23.44
		Mediterranean	21.93	24.72	23.93	25.26	24.65	23.42	25.32	23.94	23.35	24.42
		Hyper-humid	20.04	22.26	21.56	22.65	22.61	21.59	23.12	21.64	21.15	21.97

To detect the non-uniform spatial effect of climate change on temperature, the average impact of the 15 GCMs on T_{min} and T_{max} was calculated for the five climatic zones of Iran and results are summarized in Table 6. A general increase in both T_{min} and T_{max} is detected for all climatic zones. The highest increase in T_{min} corresponds to the Mediterranean climatic regions (11.2–44.5%), while the lowest one corresponds to the arid climatic regions (2.6–19%). T_{min} increment increases with time evolution. The semi-arid regions, which are the dominant climatic region of Iran, are the most vulnerable part of the country to climate change regarding T_{max} increment of 2.9–14.6%

for the future. However, the hype-arid regions will be safer under climate change since they have the lowest T_{max} increase, accounted for 1.2–9.7% compared to the base period.

Seasonal patterns of T_{min} and T_{max} variations in Figs. 10 and 11 represent the non-uniform temporal projected effect of climate change scenarios on these parameters. During 2011–2100, spring has the highest increase in T_{min} and T_{max}, while the lowest increase occurs in the autumn season for all the climatic zones. For all seasons, the highest increase in both T_{min} and T_{max} occurs in the Mediterranean climatic zone followed by the semi-arid regions. The hyper-humid
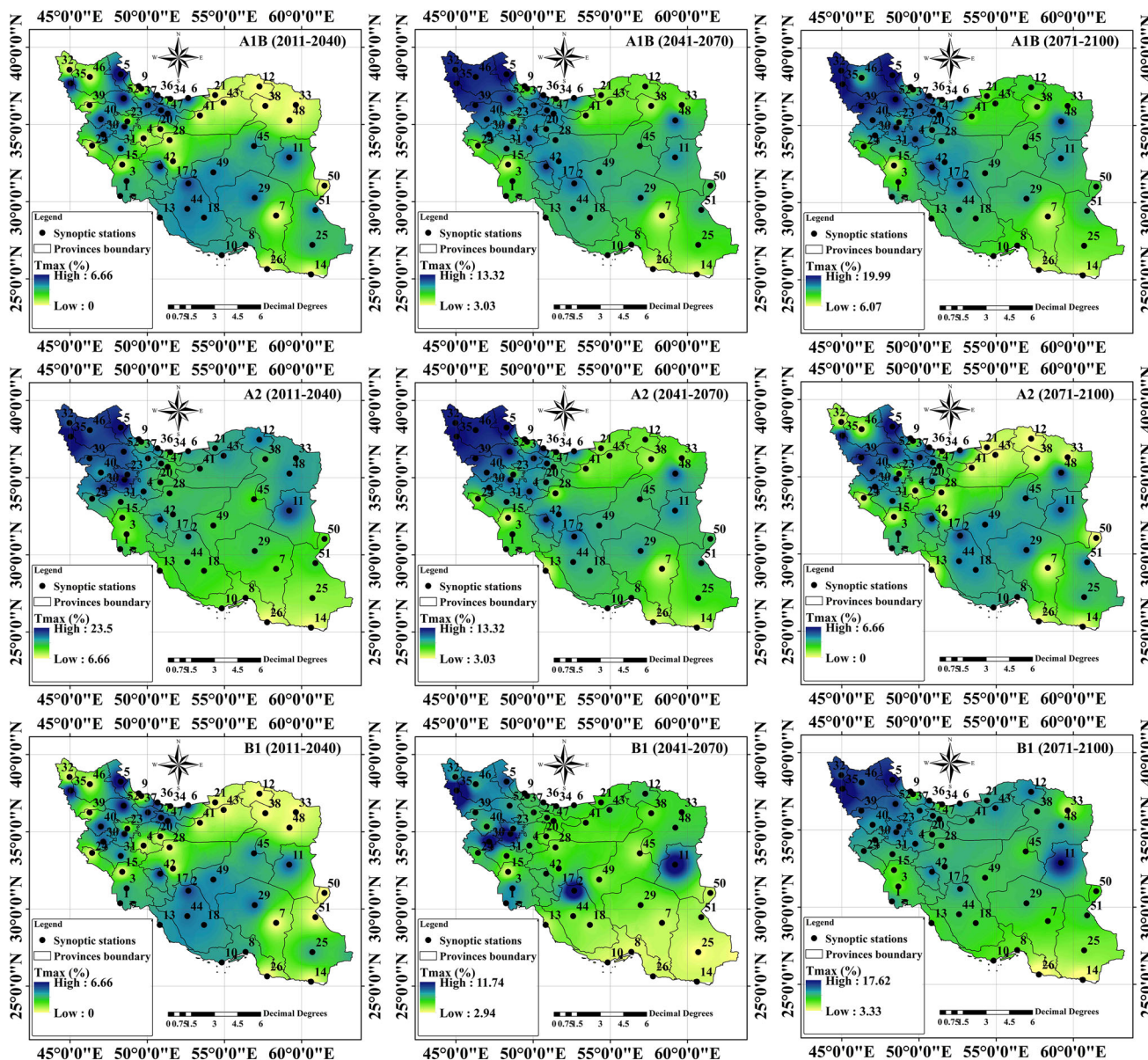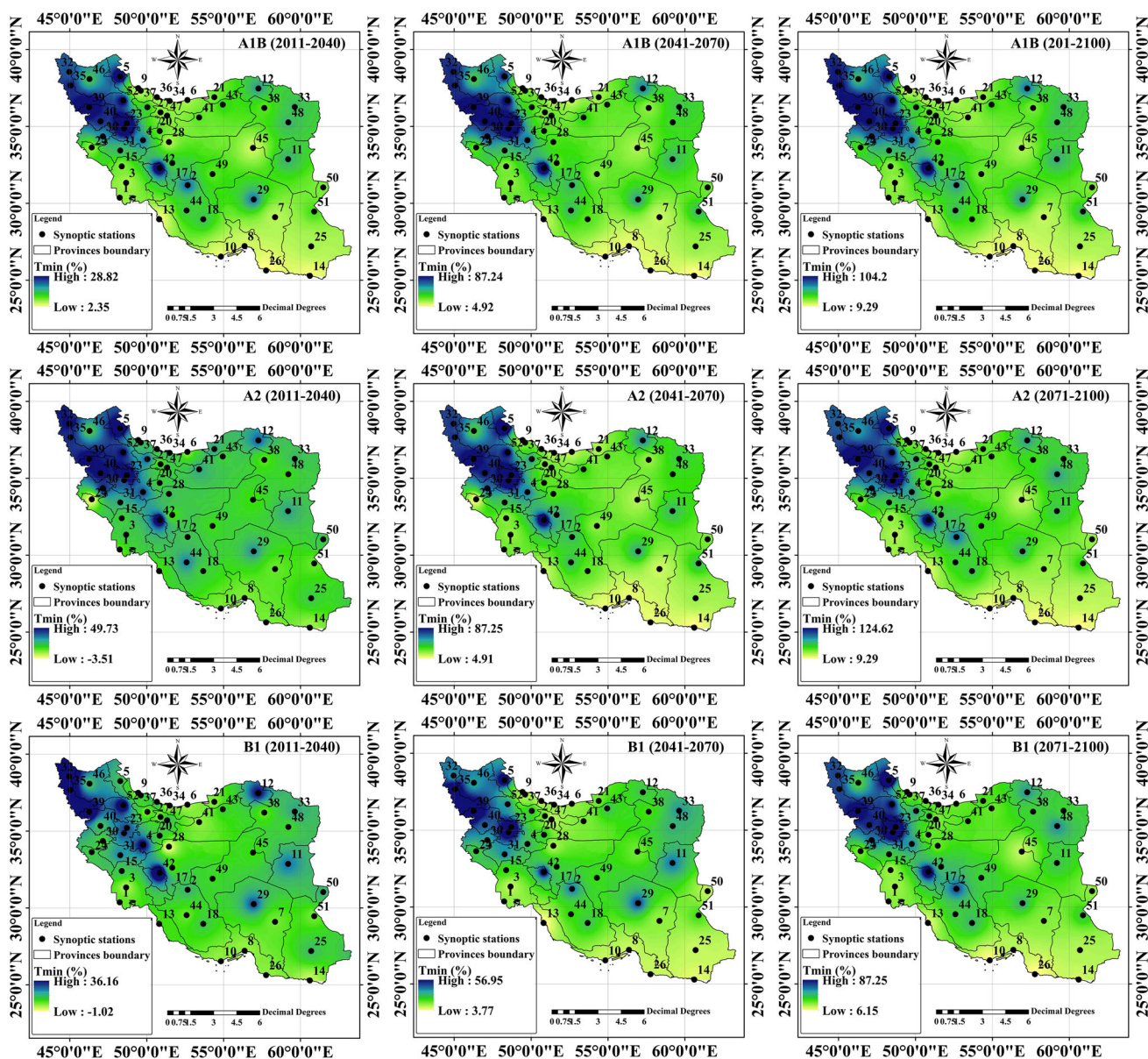
Fig. 8 Difference between T_{max} for the base and future periods as the ensemble average of the 15 GCMs under different climate change scenarios up to 2100

regions have the highest increase in seasonal T_{max}, while the arid and hyper-arid regions show the lowest increase in seasonal T_{min} and T_{max}. Increased T_{min} and T_{max} in the autumn and winter seasons may provide favorable condition for shifting the sowing dates forward. In addition, such increase may decrease the duration of the crops growing seasons since crops receive their required thermal energy in a shorter period (Karandish et al. 2016). However, increased T_{min} and T_{max} may lead to increased crop water requirement. This necesiates the investigation of climate change impact on crops to achievce a sustainable agriculture.

The range of seasonal uncertainty arising from the differences in the projections of different GCMs under the three SRES scenarios was estimated within the central 5–95% value of CDFs (i.e., CDFs represents the changes in seasonal T_{min} or T_{max} during the future periods relative to the base period). Figures 12 and 13 show the range of seasonal T_{min} and T_{max} uncertainty for different climatic zones. More uniform results are observed in seasonal T_{min} and T_{max} change compared to P. For 2011–2040, both T_{min} and T_{max} change from negative to positive, while for 2041–2070 and 2071–2100 they more likely increase

Fig. 9 Difference between T_{min} for the base and future periods as the ensemble average of the 15 GCMs under different climate change scenarios up to 2100

except for the winter season. For T_{min}, uncertainty increases for all seasons of different climatic zones in the mid- and late-century, while for T_{max} uncertainty decreases with time progress except for the Mediterranean climatic regions. Regardless of the climatic zones, the highest range of uncertainty is projected in the winter season with the lowest temperature during a year and the lowest uncertainty in the summer season with the highest T during a year. Figure 12 shows that the Mediterranean climatic regions have the highest T_{min} uncertainty, while the hyper-arid, semi-arid and arid regions have the lowest uncertainty for spring (and also winter), summer and autumn T_{min},

respectively. For all seasons, the hyper-arid regions have the lowest T_{max} uncertainty. Such results might imply that GCM uncertainty in projecting future T is larger in the humid regions. The main advantage of estimating the uncertainty range is that it provides plausible ideas about the changes that may occur in P and T in the future periods. Such knowledge will help with developing planning and coping tools and adaptation strategies. Since Iran's economy is highly dependent on agriculture, the possible effects of climate change on producing major crops are analyzed based on the obtained results for the future changes in T_{min}, T_{max} and P in the next section.
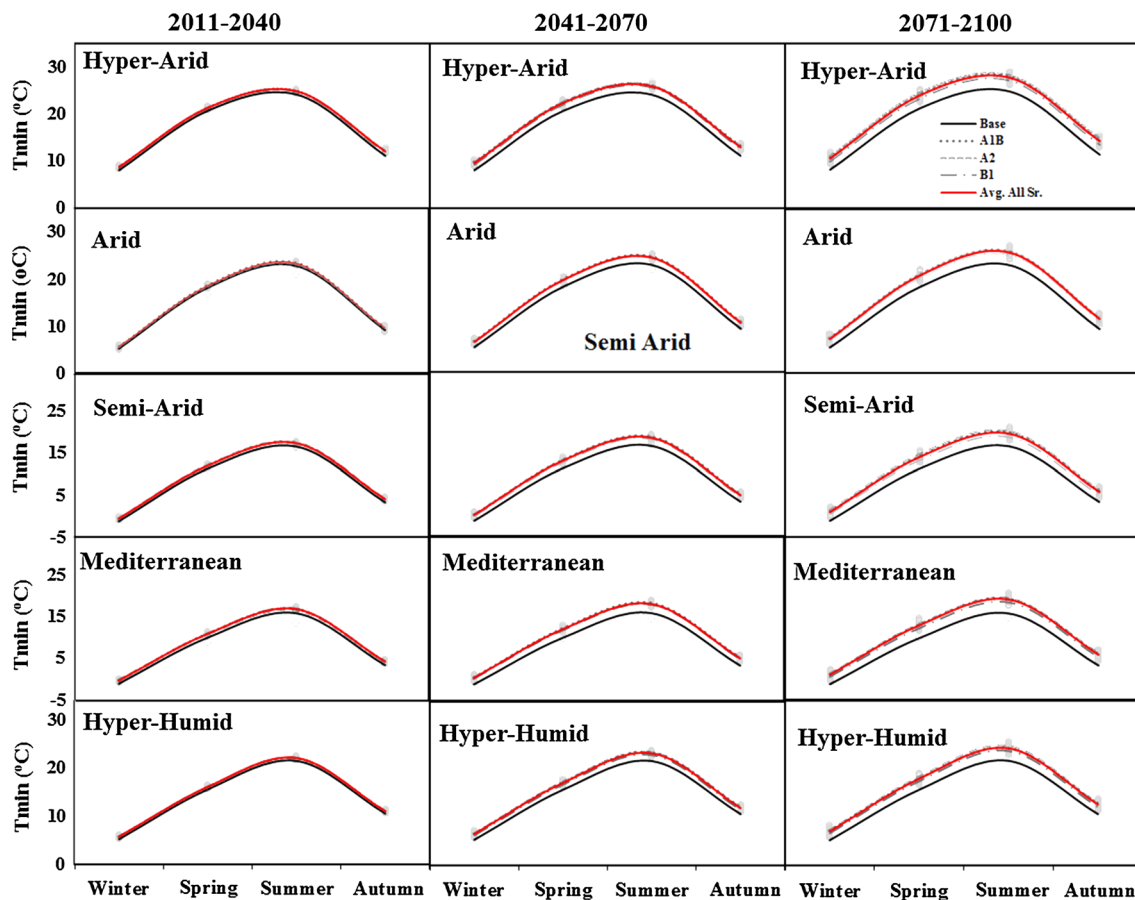
Fig. 10 Seasonal variation of T_{min} in different climatic zones under changing climate

3.4 Climate change effects on cereals in Iran

Seventy-three percentage of the agricultural land in Iran is devoted to cereals including wheat (53.82%), barley (12.24%), rice (4.59%) and maize (2.29%). 32.62% of the total agricultural production of the country is produced in these areas, of which 33% is produced in rainfed lands. Figure 14 shows the share of different provinces in producing rainfed and irrigated cereals in the country. More than 70% of the total cereal production in the country is produced in the arid and semi-arid zones in which crops are mainly produced as irrigated –crops. These climatic zones will have a considerable increase in spring and summer T_{min} and T_{max} (i.e., growing season of irrigated crops) which are key factors for crop growth. The hyper-humid climatic zone ranks second in producing rainfed cereals (14% of the total production) and seems to be less affected by global warming regarding T while autumn P will decrease during 2041–2100. Thus, agriculture in the hyper-humid regions might be threatened in the future since autumn P has a major role in the cropping cycle of rainfed

crops in these regions. In addition, there is a big threat to the food security under global warming in Iran due to its heavy dependence on irrigated agriculture which is the case for arid and semi-arid regions. On the other hand, even 53% of rainfed crops are also produced in the semi-arid climatic zone where air temperature will increase significantly in the future periods.

A crop growth simulation model, AquaCrop (FAO 2012) was used to analyze the probable effects of climate change on cereal growth in Iran. Response of irrigated cereals to climate change was simulated using the outputs of the 15 GCMs under different SRES scenarios. The probable relative changes in cereal crop water requirement (ET), yield and water use efficiency (WUE) are illustrated in Fig. 15 for the early (2011–2040), mid (2041–2070) and late (2071–2100) periods of the 21th century. A large part of the country will experience 0–30% increase in ET except for about 12% located in the west and south-west of Iran in which up to 35% reduction in ET is expected during 2011–2100. The highest increase in ET (5–28.5%) will occur in the central and northeastern parts of the
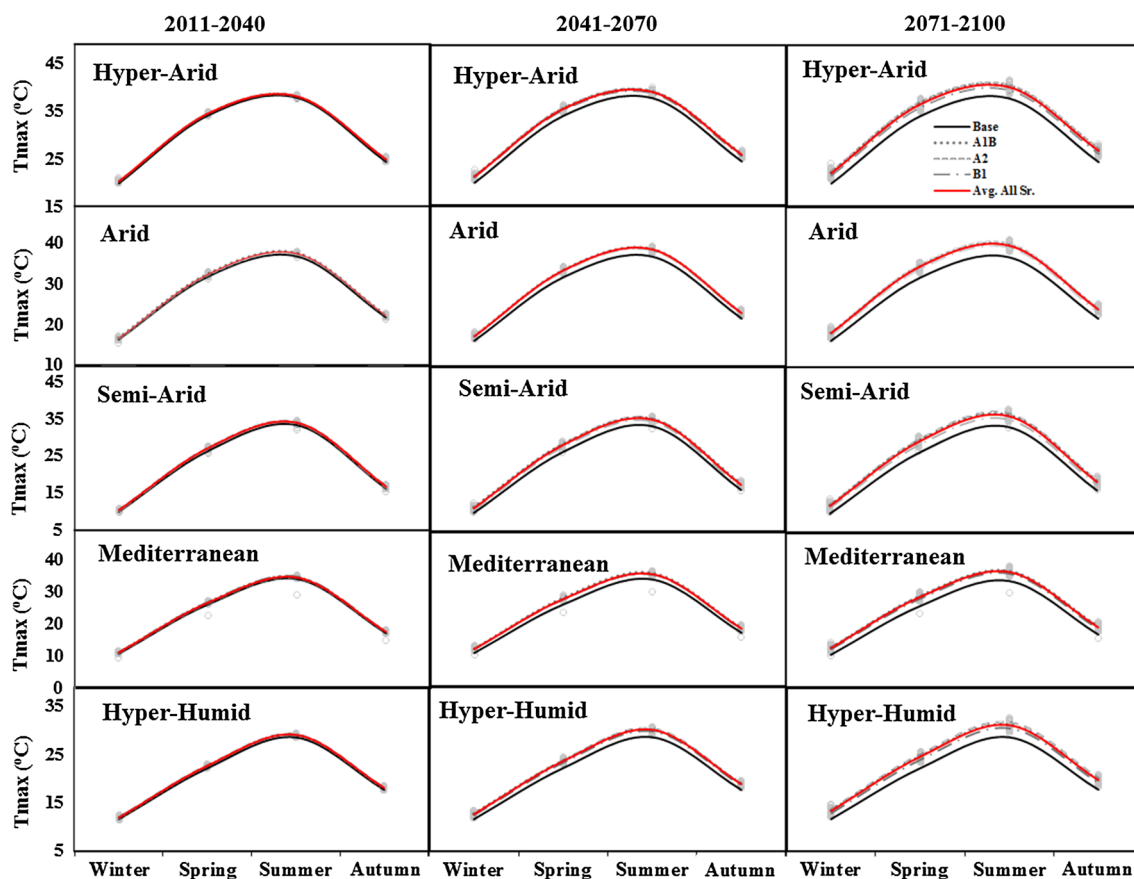
Fig. 11 Seasonal variation of T_{max} in different climatic zones under changing climate

country. A direct relationship between T and evapotranspiration has been reported in the earlier studies (Xing et al. 2014; Peterson et al. 2002). Any change in ET is expected to affect crop yield since crop yield is directly affected by root water uptake (Payero et al. 2006; Klocke et al. 2004; Stone 2003). Yield reduction in the future climate is obvious for almost 95% of the country especially in the northern-half where climate change will cause up to 15% reduction in cereal yield. Figure 15 shows that the arid and semi-arid climatic zones are more vulnerable to climate change in view of the increase in ET and decrease in crop yield, while the hyper-arid climatic zone seems to be safer.

In the province point of view, more than 50% of the total crop production in the study area is produced in six provinces, of which three provinces are located in the semi-arid climatic zone (Fars, Kermanshah and Razavi Khorasan with a share of respectively 15.8, 6.3 and 6% in the total production), one province is located in the arid climatic zone (Khuzestan with a share of 10.5% in the total production) and two provinces are located in the hyper-humid climatic zone (Golestan and Mazandaran

with a share of respectively 6.8 and 4.9% in the total production). The statistics reveal that even under the province point of view, the semi-arid climatic zone plays a major role in the total crop production of Iran. This part of the country is the most vulnerable part since it is exposed to a considerable increase in air temperature and a slight increase in P under climate change. Figure 15 also demonstrates that climate change poses a serious threat for Iran since Kermanshah, Razavi Khorasan, Khuzestan, Golestan and Mazandaran provinces are located in the northern-half of the country where the highest yield reduction under climate change is expected to occur especially during the period 2041–2070. However, cereal ET and yield in Fars province seems to be less affected which ensure a higher level of food security in this part of the country as this province is responsible for 15.8% of crop production in the country (Fig. 15).

The main reason for yield reduction under climate change could be attributed to the elevated cardinal temperatures in the future. It is known that there is a basic temperature requirement for crops to complete a specific phonological phase or the whole life cycle, whereas

Fig. 12 Range of change in seasonal and annual T_{min} under different scenarios in different climatic zones of Iran (*lower* and *upper* ends indicate respectively the 5 and 95% intervals of the uncertainty range and *dot* shows the 50% value)

extremely high and low temperature can have negative effects on crop growth, development and yield especially at critical phonological phases such as anthesis (Luo 2011). Moreover, plant growth is affected by increased T_{max} by accelerating the growth of weeds, insects and pests in warmer winters which threaten crop yield (Luo 2011). The close relation of T_{min} and T_{max} with crop yield has been demonstrated by some other researchers (e.g., Wheeler et al. 2000; Vollenweider and Gunthardt-Goerg 2005; Wahid et al. 2007). Among different crops, cereal production has been reported to be more sensitive to heat stress (Baker and Allen 1993; Stone and Nicolas 1995; Commuri and Jones 2001; Shah and Paulsen 2003; Peng et al. 2004; Ugarte et al. 2007; Selvaraj et al. 2011; Pradhan et al. 2012).

Considering that ET or crop yield alone is not adequate enough to evaluate the probable effects of climate change, water use efficiency (WUE) which takes into account both crop yield and ET was used for more comprehensive climate change impact assessment on cereals. The WUE index (kg m^{-3}) was calculated by dividing crop yield (kg ha^{-1}) by crop water requirement (m^3 ha^{-1}) for the base and future periods. The relative change in WUE was calculated for the ensemble effects of the GCMs and three SRES scenarios in the future periods (Fig. 15c). Figure 15c reveals 0–30% decrease in WUE in more than 95% of the country mainly located in the northern-half except a few spots in the western and south-west of Iran (i.e., in Fars and Ilam provinces). Also, Razavi-Khorasan, Khuzestan, Kemanshah, Golestan and Mazandaran provinces, which are responsible for about 35% of the cereal production in Iran, will experience considerable reduction in WUE (5–30%). The obtained results imply the growing threat of climate change to the national food supply in

Fig. 13 Range of change in seasonal and annual T$_{max}$ under different scenarios in different climatic zones of Iran (*lower* and *upper* ends indicate respectively the 5 and 95% intervals of the uncertainty range and *dot* shows the 50% value)

Iran, demanding further investigations for developing adaptation solutions to cope with changing climate and to sustain food and water security in the country.

4 Conclusions

In this research, annual and seasonal P, T$_{min}$ and T$_{max}$ projections were analyzed for five climatic zones in Iran based on the outputs of 15 GCMs under three SRES scenarios of A1B, A2 and B1. LARS-WG was applied to downscale data obtained from GCMs in 52 synoptic stations over the study area for early (2011–2040), mid (2041–2070) and late (2071–2100) periods of 21th century. The range of uncertainty in the projections was determined based on the 5–95% percentiles of CDFs for changes in P or T derived from different GCMs for each scenario in the

future periods compared to the base period (1981–2010). To evaluate the agriculture sustainability condition, the spatial distribution of major rainfed and irrigated crops over the country was illustrated and based on the obtained results for each climatic zone, the probable effects of climate change on cultivating these crops were analyzed using the crop growth simulation model of AquaCrop. Given results for the calibration and validation process well represent the high performance of LARS-WG for simulating climatic variables for all stations. For 2011–2100, the majority of GCMs as well as the median values of the 15 GCMs for each scenario show a positive change in both annual and seasonal P. The highest increase (11.2–44.5%) in T$_{min}$ occurred in the Mediterranean climatic regions followed by the semi-arid regions. Rainy seasons as well as the hyper-humid regions have the highest P uncertainty, while the summer season and the hyper-arid regions show
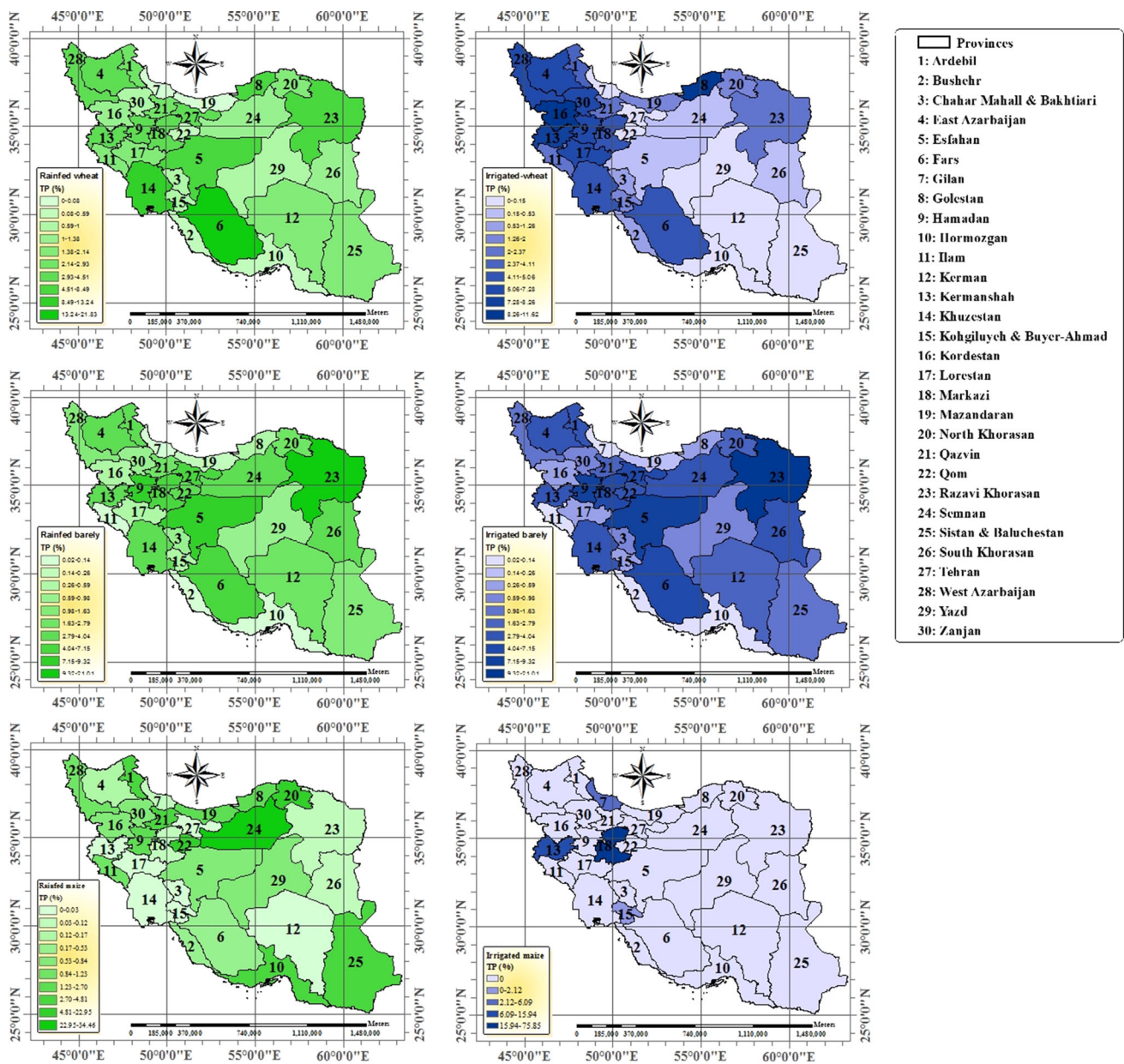
Fig. 14 Share of different provinces in producing rainfed and irrigated cereals in Iran

the lowest uncertainty in cardinal T (i.e., both T_{min} and T_{max}).

Uncertainty analysis reveals that there is a high probability that the change in annual and seasonal cardinal T may be positive during the irrigated crops' growing seasons especially for the semi-arid climatic zones which are responsible for producing a considerable share of agricultural products. As cereals are the major crops grown in the country and their yield is highly dependent on thermal condition during the growing seasons, the effect of climate change on cereals was investigated. The elevated T beyond

the favorable thresholds significantly reduces the cereal's yield up to 15% and thereby, Iran's food security. Water security is also threatened since cereal WUE will decrease up to 30 in 95% of the country. Coping with such probable hazards for achieving sustainable agriculture requires planning suitable adaptation solutions to save humankind being in the future climate. Cultivating high-tolerant and early cultivars as well as spatially prioritizing crop cultivation could be some examples of these solutions which might help with saving food and water security under changing climates. Overall, further investigations are
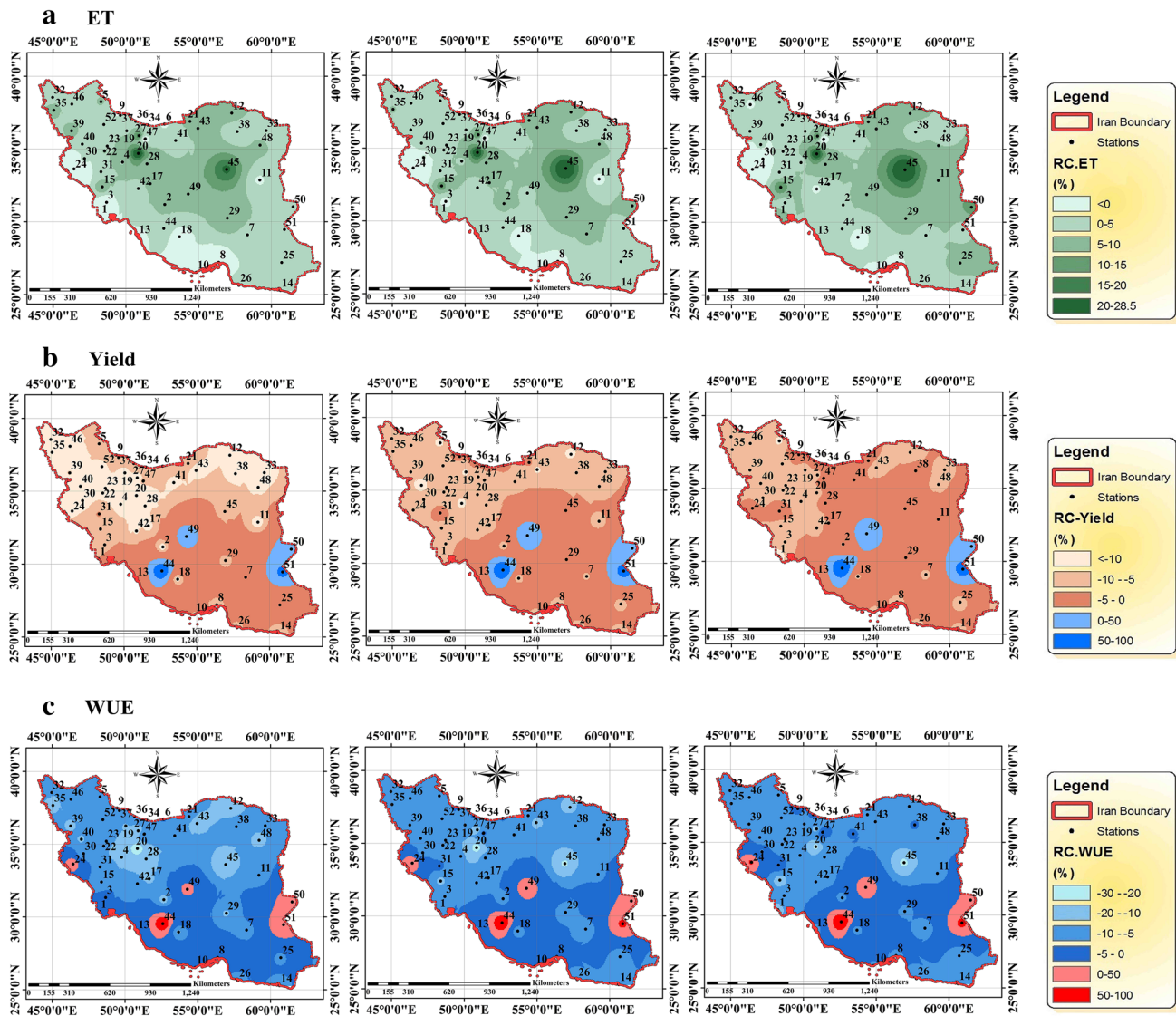
Fig. 15 Relative change in cereal water requirement (a), yield (b) and water use efficiency (c) under climate change based on the average results of the 15 GCMs for all scenarios in the future periods compared to the base period

highly recommended to propose possible solutions for achieving sustainable agriculture under climate change in the water-scarce arid regions such as Iran.

References

Abahussain AA, Abdu AS, Al-Zubari WK, El-Deen NA, Raheen MA (2002) Desertification, in the Arab region: analysis of current status and trends. J Arid Environ 51:521–545

Abbaspour CK, Faramarzi M, Seyed Ghasemi S, Yong H (2009) Assessing the impact of climate change on water resources in Iran. Water Res 45:1–16

Agarwal A, Babel MS, Maskey SH (2014) Analysis of future precipitation in the Koshi river basin, Nepal. J Hydrol 513:422–434

Aldaya M, Allan J, Hoekstra A (2010) Strategic importance of green water in international crop trade. Ecol Econ 69:887–894

Alizade A, Sayyari N, Hesami Kermani MR, Banayan Avval M, Farid Hosseini E (2010) Assessment of effects of climate change on water resources and agriculture water using water. Soil J 24:815–835

Almasi P, Soltani S (2016) Assessment of the climate change impacts on flood frequency. Stoch Environ Res Risk Assess. doi:10.1007/s00477-016-1263-1

Azarakhshi M, Farzadmehr J, Eslah M, Sahabi H (2013) An investigation trends of annual and seasonal rainfall and temperature in different climatologically regions of Iran. J Range Watershed Manag 66(1):1–16

Baker JT, Allen LH (1993) Contrasting crop species responses to CO_2 and temperature: rice, soybean, and citrus. Vegetatio 104(105):239–260

CCSP (2008) Climate models: an assessment of strengths and limitations. In: A Report by the U.S. Climate Change Science Program and the Subcommittee on Global Change Research.

Department of Energy, Office of Biological and Environmental Research, Washington, DC

Chen J, Brissette FP, Leconte R (2011) Uncertainty of downscaling method in quantifying the impact of climate change on hydrology. J Hydrol 401:190–202

Chen H, Gue J, Zhang Z, Xu CY (2013) Prediction of temperature and precipitation in Sudan and South Sudan by using LARS-WG in future. Theor Appl Climatol 113:363–375

Christensen J, Hewitson B, Busuioc A, Chen A, Gao X, Held I, Jones R, Kolli R, Kwon WT, Laprise R, Rueda VM, Mearns L, Menéndez C, Räisänen J, Rinke A, Sarr A, Whetton P (2007) Regional climate projections. In: Solomon S, Qin D, Manning M, Chen Z, Marquis M, Averyt KB, Tignor M, Miller HL (eds) Climate change 2007: the physical science basis. Contribution of Working Group I to the Fourth Assessment Report of the Intergovernmental Panel on Climate Change, Cambridge University Press, Cambridge, UK

Commuri PD, Jones RD (2001) High temperatures during endosperm cell division in maize: a genotypic comparison under in vitro and field conditions. Crop Sci 41:1122–1130

Dastorani MT, Poormohammadi S (2012) Evaluation of the effects of climate change on temperature, precipitation and evapotranspiration in Iran. In: International Conference on Applied Life Sciences, Turkey, 2012, pp 73–79

Enete AA, Amusa TA (2010) Challenges of agricultural adaptation to climate change in Nigeria: a synthesis from the literature, Field Actions Science Reports. http://factsreports.revues.org/678

Etemadi H, Samadi SZ, Sharifikia M (2012) Statistical downscaling of climatic variables in Shadegan Wetland Iran. Earth Sci Clim Chang 1:508. doi:10.4172/scientificreports.508

Etemadi H, Samadi S, Sharifikia M (2014) Uncertainty analysis of statistical downscaling models using general circulation model over an international wetland. Clim Dyn 42:2899–2920

Evans J, Geerken R (2004) Discrimination between climate and human-induced dryland degradation. J Arid Environ 57:535–554

FAO (2012) AquaCrop reference manual. FAO, Land and Water Division Rome, Italy

Fowler HJ, Blenkinsop S, Tebaldi C (2007) Linking climate change modeling to impact studies: recent advances in downscaling techniques of hydrological modeling. Int J Climatol 27:1547–1578

Ghahraman B (2006) Time trend in the mean annual temperature of Iran. Turk J Agric For 30:439–448

Gil-Alana LA (2012) Long memory, seasonality and time trends in the average monthly temperatures in Alaska. Theor Appl Climatol 108:385–396

Girvetz EH, Zganjar C, Raber GT, Maurer EP, Kareiva P (2009) Applied climate-change analysis: the climate wizard tool. PLoS ONE 4(12):e8320. doi:10.1371/journal.pone.0008320

Goodarzi E, Dastorani M, Massah Bavani A, Talebi A (2015) Evaluation of the change-factor and LARS-WG methods of downscaling for simulation of climatic variables in the future (case study: Herat Azam Watershed, Yazd—Iran). Ecopersia 3(1):833–846

Goyal RK (2004) Sensitivity of evapotranspiration to global warming: a case study of arid zone of Rajasthan (India). Agric Water Manag 69:1–11

Hamdi MR, Abu-Allaban M, Al-Shayeb A, Jaber M, Momani NM (2009) Climate change in Jordan: a comprehensive examination approach. Am J Environ Sci 5(1):58–68

Hashmi MZ, Shamseldin AY, Melville BW (2011) Comparison of SDSM and LARS-WG for simulation and downscaling of extreme precipitation events in a watershed. Stoch Environ Res Risk Assess 25:475–484

Haskett JD, Pachepsky YA, Acock B (2000) Effect of climate and atmospheric change on soybean water stress: a study of Iowa. Ecol Model 135(2–3):265–277

Hewitson BC, Crane RG (1996) Climate downscaling: techniques and application. Clim Res 7:85–95

IPCC (2007) Summary for policymakers. In: Solomon S, Qin D, Manning M, Chen Z, Marquis M, Averyt KB, Tignor M, Miller HL (eds) In climate change 2007: the physical science basis. Contribution ofWorking Group I to the Fourth Assessment Report of the Intergovernmental Panel on Climate Change. Cambridge University Press, Cambridge, UK

Karandish F (2016) Improved soil-plant water dynamics and economic water use efficiency in a maize field under locally water stress. Arch Agron Soil Sci 62(9):1311–1323

Karandish F, Kalanaki M, Saberali SF (2016) Projected impacts of global warming on cropping calendar and water requirement of maize in a humid climate. Arch Agron Soil Sci. doi:10.1080/03650340.2016.1177176

Kazemi-Rad L, Mohammadi H (2015) Climate change assessment in Gilan Province, Iran. Int J Agric Crop Sci 8(2):86–93

Kendall MG (1975) Rank correlation methods. Griffin, London.

Klocke NL, Schneekloth JP, Melvin S, Clark RT, Payero JO (2004) Field scale limited irrigation scenarios for water policy strategies. Appl Eng Agric 20:623–631

Knutti R, Stocker TF, Joos F, Plattner GK (2003) Probabilistic climate change projections using neural networks. Clim Dyn 21:257–272

Konar M, Dalin C, Hanasaki N, Rinaldo A, Rodriguez-Iturbe I (2012) Temporal dynamics of blue and green virtual water trade netweork. Water Resour Res 48:1–11

Luo Q (2011) Temperature threshold and crop production: a review. Clim Chang 109:583–598

Luo Q (2016) Necessity for post-processing dynamically downscaled climate projections for impact and adaptation studies. Stoch Environ Res Risk Assess. doi:10.1007/s00477-016-1233-7

Mann HB (1945) Nonparametric tests against trend. Econometrica 13:245–259

Minville M, Brissette F, Leconte R (2008) Uncertainty of the impact of climate change on the hydrology of a nordic watershed. J Hydrol 358:70–83

Modarres R, da Silva VPR (2007) Rainfall trends in arid and semi-arid regions of Iran. J Arid Environ 70:344–355

Nazemosadat MJ, Samani N, Barry DA, Molaii Niko M (2006) ENSO forcing on climate change in Iran: precipitation analyses. Iran J Sci Technol Trans B 30(B4):47–61

Osman Y, Al-Ansari N, Abdellatif M, Aljawad SB, Knutsson S (2014) Expected future precipitation in central Iraq using LARS-WG stochastic weather generator. Engineering 6:948–959

Ouyang F, Lu H, Zhu Y, Zhang J, Yu Z, Chen X, Li M (2014) Uncertainty analysis of downscaling methods in assessing the influence of climate change on hydrology. Stoch Environ Res Risk Assess 28:991–1010

Partal T, Kahya E (2006) Trend analysis in Turkish precipitation data. Hydrol Process 20:2011–2026

Payero JO, Melvin SR, Irmak S, Tarkalson D (2006) Yield response of corn to deficit irrigation in a semiarid climate. Agric Water Manag 84:101–112

Peng S, Huang J, Sheehy JE, Lanza RC, Visperas RM, Zhong X, Centeno GS, Khush GS, Cassman KG (2004) Rice yields decline with higher night temperatures from global warming. Proc Natl Acad Sci USA. http://www.pnas.org/cgi/content/full/101/27/9971

Peterson TC, Golubev VS, Groisman PY (2002) Evaporation losing its strength. Nature 377:687–688

Pradhan GP, Prasad PVV, Fritz AK, Kirkham MB, Gill BS (2012) High temperature tolerance in *Aegilops* species and its potential transfer to wheat. Crop Sci 52:292–304

Randall DA, Wood RA, Bony S, Colman R, Fichefet T, Fyfe J, et al. (2007) Cilmate models and their evaluation. In: Climate change 2007: the physical science basis. Contribution of Working Group I to the ARIV of IPCC. Cambridge University Press, Cambridge, UK

Raziei T, Daneshkar Arasteh P, Saghfian B (2005) Annual rainfall trend in arid and semi-arid regions of Iran. In: ICID 21st European Regional Conference, Germany

Reddy KS, Kumar M, Maruthi V, Umesha B, Vijayalaxmi, NageswarRao CVK (2014) Climate change analysis in southern Telangana region, Andhra Pradesh using LARS-WG model. Curr Sci India 107(1):54–62

Sarker MAR, Alam K, Gow J (2012) Exploring the relationship between climate change and rice yield in Bangladesh: An analysis of time series data. Agricultural System, Elsevier Ltd., pp 11–16

Selvaraj IC, Nagarajan P, Thiyagarajan K, Bharathi M, Rabindran R (2011) Genetic parameters of variability, correlation and path coefficient studies for grain yield and other yield attributes among rice blast disease resistant genotypes of rice (*Oryza Sativa L.*). Afr J Biotechnol 10:3322–3334

Semenov MA, Barrow EM (2002) A stochastic weather generator for use in climate impact studies. User's manual, Version 3.0

Semenov MA, Stratonovitch P (2010) Use of multi-model ensembles from global climate models for assessment of climate change impacts. Clim Res 41(1):1–14

Sen PK (1968) Estimates of the regression coefficient based on Kendall's tau. J Am Stat Assoc 63(324):1379–1389

Shah NH, Paulsen GM (2003) Interaction of drought and high temperature on photosynthesis and grain-filling of wheat. Plant Soil 257:219–226

Smadi MM (2006) Observed abrupt changes in minimum and maximum temperatures in Jordan in the 20th century. Am J Environ Sci 2(3):114–120

Stone LR (2003) Crop water use requirements and water use efficiencies. In: Proceedings of the 15th annual Central Plains Irrigation Conference and Exposition, Colby, Kansas, pp. 127–133

Stone PJ, Nicolas ME (1995) Effect of timing of heat stress during grain filling on two wheat varieties differing in heat tolerance. I. Grain growth. Aust J Plant Physiol 22:927–934

Tabari H, Talaee Hosseinzadeh P (2011) Temporal variability of precipitation over Iran: 1966–2005. J Hydrol 396(3):313–320

Tabari H, Marofi S, Hosseinzadeh Talaee P, Mohammadi K (2011) Trend analysis of reference evapotranspiration in the western half of Iran. Agric For Meteorol 151(2):128–136

Tabari H, Hosseinzadeh Talaee P, Mousavi Nadoushani SS, Willems P, Marchetto A (2014) A survey of temperature and precipitation based aridity indices in Iran. Quat Int 345:158–166

Tabari H, Taye MT, Willems P (2015) Water availability change in central Belgium for the late 21st century. Glob Planet Chang 131:115–123

Ugarte C, Calderini DF, Slafer GA (2007) Grain weight and grain number responsiveness to preanthesis temperature in wheat, barley and triticale. Field Crop Res 100:240–248

Vollenweider P, Gunthardt-Goerg MS (2005) Diagnosis of abiotic and biotic stress factors using the visible symptoms in foliage. Environ Pollut 137:455–465

Wahid A, Gelani S, Ashraf M, Foolad MR (2007) Heat tolerance in 1260 plants: an overview. Environ Exp Bot 61:199–223

Wheeler TR, Craufurd PQ, Ellis RH, Porter JR, Vara Prasad PV (2000) Temperature variability and the yield of annual crops. Agric Ecosyst Environ 82:159–167

Wilby RL (1999) The weather generation game: a review of stochastic weather models. Prog Phys Geogr 23(3):329–357

Wilby RL, Charles SP, Zorita E, Timbal B, Whetton P, Mearns LO (2004) Guidelines for use of climate scenarios developed from statistical downscaling methods. Supporting material of the Intergovernmental Panel on Climate Change, available from the DDC of IPCC TGCIA 27

Xing W, Weiguang W, Quanxi S, Shizhang P, Zhongbo Y, Bin Y, John T (2014) Changes of reference evapotranspiration in the Haihe River Basin: present observations and future projection from climatic variables through multi-model ensemble. Glob Planet Chang 115:1–15

Xu CY (1999) From GCMs to river flow: a review of downscaling methods and hydrologic modelling approaches. Prog Phys Geogr 23:229–249

Yang H, Wang L, Abbaspour K, Zehnder A (2006) Virtual water trade: an assessment of water use efficiency in the international food trade. Hydrol Earth Syst Sci 10:443–454

Yu PS, Yang TC, Chou CC (2002) Effects of climate change on evapotranspiration from paddy fields in southern Taiwan. Clim Chang 54:165–179

Zhang X, Xu YP, Fu G (2014) Uncertainties in SWAT extreme flow simulation under climate change. J Hydrol 515:205–222. doi:10.1016/j.jhydrol.2014.04.064

Zickfeld K, Knopf B, Petoukhov V, Schellnhuber HJ (2005) Is the Indian summer monsoon stable against global change? Geophys Res Lett 32:L15707